The research reported herein was supported wholly by the U.S. Public Health Service (NIH) Grant GM 13756-01.

The research reported herein was supported wholly by the U.S. Public Health Service (NIH) Grant GM 13756-01.

FIELD EMISSION SOURCES FOR SCANNING ELECTRON MICROSCOPY

by

P. J. Le May

Memorandum No. ERL-M200

21 December 1966

ELECTRONICS RESEARCH LABORATORY

College of Engineering
University of California, Berkeley
94720

ABSTRACT

This is a study of field emission tips. Particular emphasis is placed on the fabrication of the tips, which involved much time and alteration of method. Tips have been reliably made to specification and tested. The tests offer data which agree with field emission theory and indicate that the tips can be used in a scanning electron microscope.

ACKNOWLEDGMENTS

I would like to thank John Weisner for use of his etch circuit and Noel MacDonald for taking Scanning Electron Microscope photographs of our tips. I owe a special debt to my research advisor, Daniel Weiner, without whose ideas and advice this thesis could not have come about.

TABLE OF CONTENTS

LIST OF FIGURES

LIST OF FIGURES (Cont'd.)

I. INTRODUCTION

When a piece of cold metal is placed in an electric field, electrons are emitted from its surface. The electric field must be $\geq 3(10^7)$ V/cm for this process to occur appreciably. The process is called field emission. At lower fields, the metal has to be heated in order that it emit a significant number of electrons. The heated electron emission is called thermionic emission. When the metal is both heated and placed in a strong electric field, a combined process, known as T-F emission, occurs (1, p. 90). In this latter process, the temperature is less than that required for thermionic emission, while the electric field is less than that required for field emission. The temperature and field ranges of T-F emission are given more completely in the literature (2, p. 14).

The process of field emission was discovered by Wood in 1897. Schottky tried, in 1923, to explain it by applying a refined classical theory, but it was not until 1928 that Fowler and Nordheim developed a successful explanation with wave mechanics. They found the current density (J) to be a function of the field (F) and the work function (ϕ) of the metal. The form of their equation is:

$$J = (A_1 F^2/\phi) \exp\left[A_2 \phi^{3/2} f(y)/F\right] ,$$

where the constants are given (using the corrections of Burgess, Kroemer, and Houston) (1, p. 94) as:

$$A_1 = 1.54(10^{-6}) \qquad (\text{amp/volt}^2)\text{eV}, \tag{1}$$

and $$A_2 = -6.83(10^7) \qquad (\text{V/cm})\text{eV}^{-3/2} \tag{2}$$

J is in amp/cm^2, F in V/cm, and ϵ is the kinetic energy of the electrons in eV. f(y) is a tabulated function (1, p. 93) of the dimensionless variable:

$$y = 3.79(10^{-4})\, F^{1/2}/(\phi - \epsilon). \tag{3}$$

Since neither J nor F are directly measurable quantities, it will be convenient to derive an expression relating the current (I) and voltage (V) from the previous relation using:

$$I = \int J\, dA \qquad \text{and} \qquad F = \beta V. \tag{4}$$

The current density is integrated over the surface of the emitting area, and β is a purely geometrical quantity which we will discuss later. If the emitting area and the work function are approximately constant, they can be represented by effective values, thus;

$$I = JA_e = (A_1 \beta^2 V^2/\phi_e)\, A_e \exp\left[A_2 \phi_e^{3/2} f(y)/\beta V\right]. \tag{5}$$

If everything but V is constant, this can be further approximated as:

$$I = A_3 e^{-A_4/V} . \qquad (6)$$

This relation was discovered empirically by Milikan and Lauritsen (3, p. 45). Thus, for field emission, a plot of ln I vs 1/V should yield a straight line, and such plots will constitute the main experimental results of this paper.

Equation 5 is approximately correct for current densities below $\sim 6(10^6)$ amp/cm^2 . At higher current densities, space-charge effects alter the relationship significantly (1, p. 109).

Various methods have been used to calculate the geometrical factor β ; for example, by solving Laplace's equation for idealized equipotentials (representing the tip as a sphere on a cone, the anode as a plane). However, we will use the empirical formula derived by Dyke (3, p. 11):

$$\beta = 1.7/(r^{0.87} R^{0.13} \alpha^{1/3}) , \qquad \text{cm}^{-1} \qquad (7)$$

The quantities r, R, and α are displayed (Fig. 1). As can be seen from Eq. 7, β is essentially independent of the anode geometry.

The effective emitting area (A_e) is a function of the field (F). This dependence has been calculated by Dyke (4, p. 15).

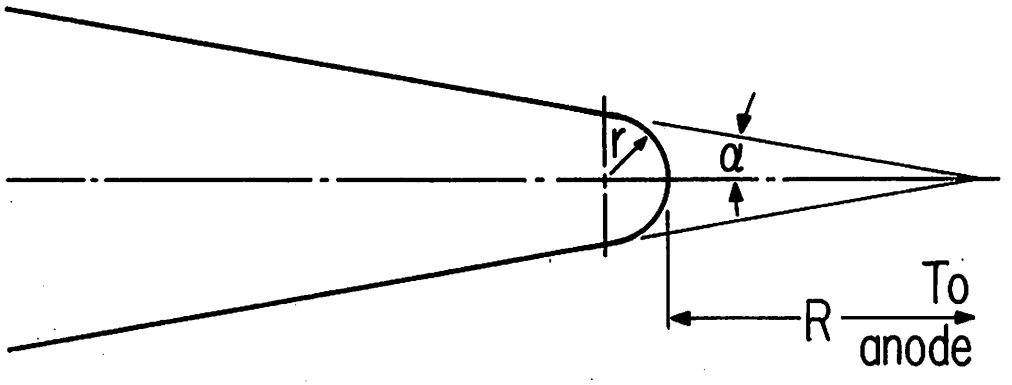

Fig. 1. The field emission tip

For use as an electron source, the cold field emission cathode has certain advantages over the common thermionic emission cathode. It can be made as small as 100 $\mathring{A}$ and can carry current densities higher by at least a factor of 10^3 (2, p. 15). Also, it does not need continuous heating. The biggest disadvantage is that a high vacuum is required for stability (10^{-7} torr). This requirement, however, can be lowered if the cathode is heated (i.e., $100^\circ \rightarrow 1800^\circ$C).

Ion sputtering tends to dull the emitter tips, thus reducing the field emission current at a given voltage. The rate of reduction is proportional to the gas pressure and can hence be used to estimate the pressure. Martin et al. (4, p. 24) give an empirical formula for this:

$$(1/I)dI/dt = 10^{11} pI^{0.7}, \tag{8}$$

where I is the current in amperes, t the time in hours, and p the partial pressure of helium expressed as the equivalent nitrogen pressure in mm Hg indicated by an ionization gauge.

The field emission cathode has the properties of small size combined with high current density that make it advantageous for scanning electron microscopy. Its small size means less demagnification and thus a simpler lens system. Its high current density means that pictures can be taken in less time, allowing less electrical and mechanical stability. The particular requirements to be met for the scanning

electron microscope in construction here are that the tips must (1) emit 10^{-5} amp of current at 10 kV, which implies a tip radius of about 0.7 microns, (2) emit the electrons peaked in the forward direction, (3) exhibit reliability in fabrication, and (4) have a lifetime of several hours.

II. PROCEDURE FOR FABRICATING THE FIELD EMISSION TIPS

The field emitter must be both small and strong. The smaller the emitting point, the greater is the field for a particular voltage (Eq. 4), and the tip must be strong enough to support itself rigidly. Tungsten wire of about 5 mil diameter serves as a good emitter. The point is formed on the wire by an electrolytic etch.

The crystal orientation of the tungsten wire must be considered since the intensity of emission is anisotropic. The anisotropy results from variations in the number of near-neighbor bonds and the packing density of the tungsten atoms at the tip surface (1, p. 135). High purity single-crystal tungsten wire oriented in the ⟨310⟩ direction is available (Field Emission Corporation) but is expensive (~ $125/in.). Regular tungsten wire, 4 or 5 mils in diameter and oriented in the ⟨110⟩ direction, was used. It required annealing in a Balzer vacuum system at 2300°K → 2800°K for about 48 hours. The temperature measurements were made with an optical pyrometer. The large error in temperature measurement was due mainly to the small area of the hot surface. Fortunately, higher accuracy was not needed here.

The field emission tip must be mounted in such a way that it can be heated and brought to a high negative potential. Two different methods have been used. The first is with a Kovar-glass base (Fig. 2). A 2-cm loop of untreated tungsten wire (4 or 5 mils diameter) is formed and its ends placed through the insulated holes in the base. Two lengths of copper wire (23 mils diameter) are then put into the holes such that the tungsten loop is securely wedged; the diameter of the holes is only slightly larger than that of the copper. Soldered connections are then made between the Kovar and copper leads on both sides of the base. The second method makes use of 23 mil diameter Monel wire leads with an epoxy insulation applied between them (Fig. 3). The 2 cm by 4 - 5 mil tungsten loop is then spot-welded to the Monel. Monel was used since it is easy to spot-weld tungsten to it. The epoxy is a low vapor pressure type (Torr-Seal) specially manufactured for use in a vacuum.

A comparison of these two methods shows that the epoxy-Monel mounting is better. The advantages are: (1) spot-welded tungsten-Monel makes a better electrical connection than the tungsten-copper mechanical wedge used with the Kovar glass, (2) the epoxy-Monel mounting is simpler to construct, and (3) less capacitive effects arise with the use of epoxy than with the use of Kovar. The main disadvantage is poorer strength; the protruding Monel wires are not as rigid as the Kovar-glass base. Also, care must be taken not to heat the

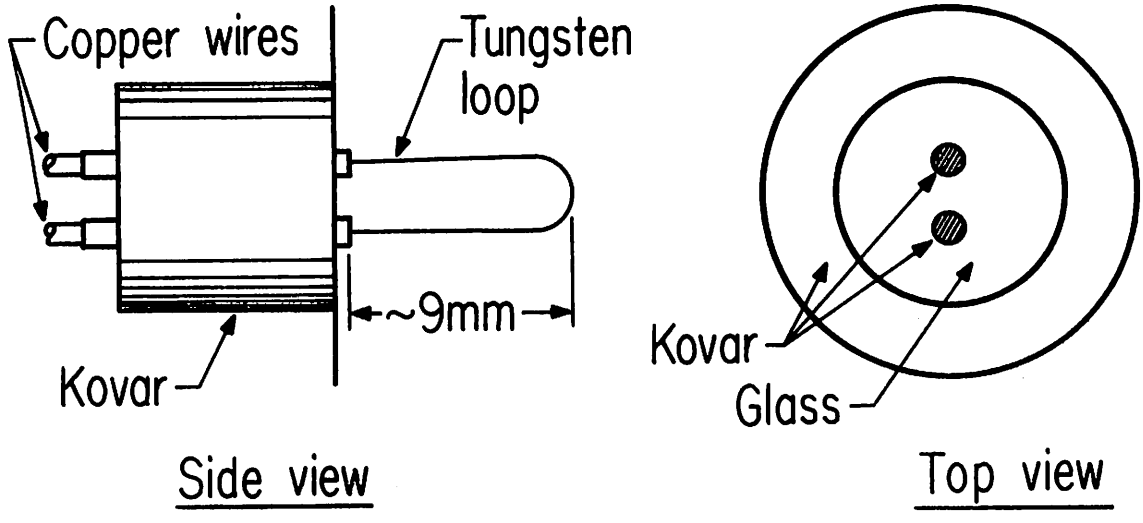

Fig. 2. Kovar-glass base

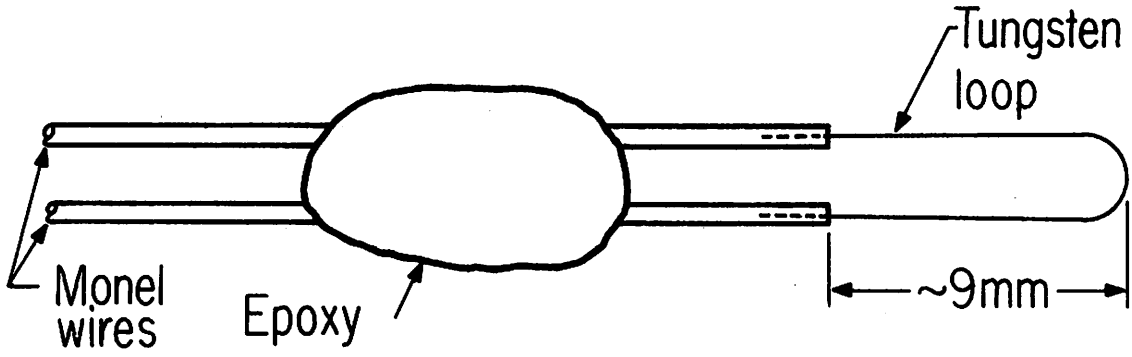

Fig. 3. Epoxy - monel base

epoxy for prolonged periods as it tends to decompose at high temperatures.

The tungsten tip must now be spot-welded to the loop. Due to the small size of the wires and the difficulty of making a good tungsten-tungsten weld, this is the most difficult part of the procedure.

The spot welder, designed for heavier work, was set at its lowest settings (shortest time pulse, lowest voltage), and tape or paper spacers were used to prevent the tungsten wires from being pressed through one another upon heating. These spacers are made such that they are just a little thinner than the sum of the loop and tip wire diameters. The lower electrode was placed in a cork which supported the loop and its holder, the tip wires and the symmetrically placed spacers. This greatly facilitated welding reliability (Fig. 4). A section of wire, 3 1/2 - 4 mm, is cut to make the tip and is then welded to the end of the loop. At first, the ⟨ 110 ⟩ tungsten wire was put on parallel to the axis of the loop holder (Fig. 5a). Afterwards, it was decided to orient the wire at an angle of 15 - 20^{o} from this direction (Fig. 5b) to take advantage of the emission properties of ⟨ 110 ⟩ wire (1, p. 133). The ⟨ 310 ⟩ tips should be put on parallel to the axis since the ⟨ 310 ⟩ direction is that in which emission is greatest. The pressure on the weld by the electrodes is controlled by a foot pedal, and it is the crudeness of this control that accounts for the unsuccessful welds. If

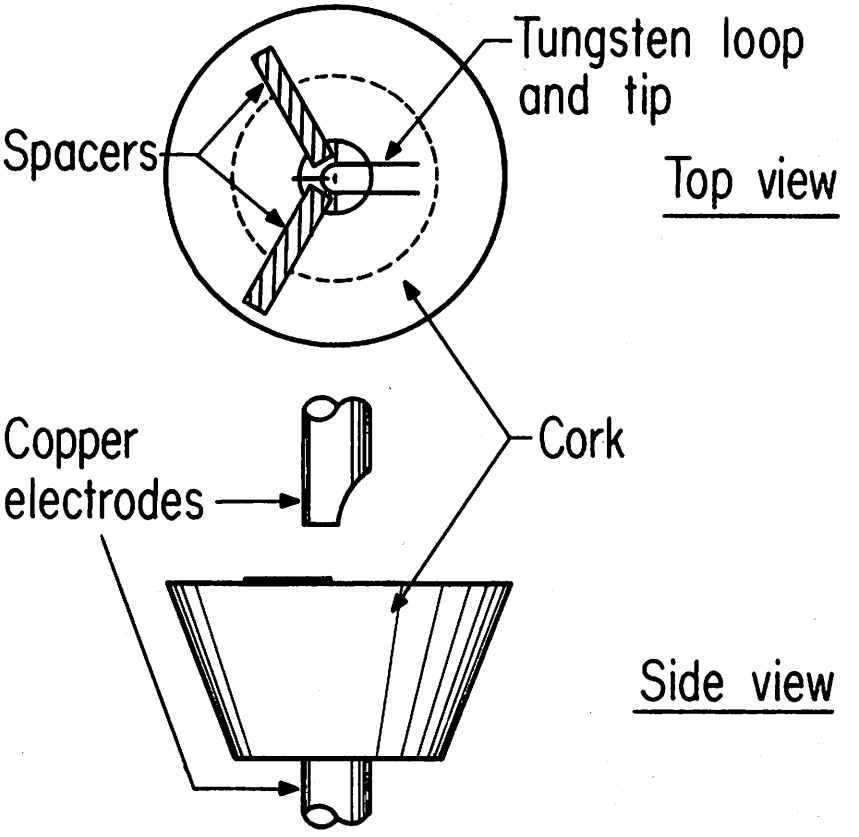

Fig. 4. Electrode apparatus for tungsten-tungsten spotweld

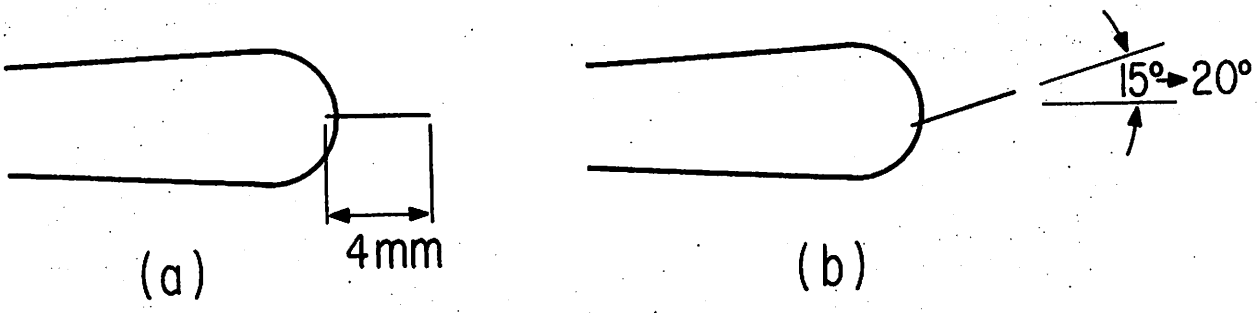

Fig. 5. Tungsten tip on tungsten loop

the pressure is too small, the current may arc and cause too much heating and subsequent breakage of either the loop or the tip. If the pressure is too great, there may be breakage from mechanical strain. The probability of success has been increased by a little practice from 25 to 80%.

Since the ⟨ 310 ⟩ material is expensive, an effort is made to reuse the tips that fail to weld. In most cases this is possible since it is usually the loop that breaks.

To form a sharp field emission point (100 - 1000 Å), electrolytic etching has been shown to be the best method (1, p. 172). The electrolytic etch apparatus is shown in Fig. 6. Before a point is formed, however, the tip must be cleaned. This was done with acetone. The etching occurs to a greater degree at the meniscus due to the convection currents and subsequent replenishment of solution at this point. Because of this, the tungsten wire becomes thinnest at the surface and finally breaks there by tensile failure caused by the weight of the material below the surface. A very sharp tip is formed at the point of breakage. Since there is an etching of any material left in solution, the current must be shut off within a few milliseconds after tensile failure or the tip will dull to an undesirable degree. (It has subsequently been suggested by Dr. S. Ranganathan that by rapidly rotating the tip one can obtain a spherical rather than ellipsoidal point.)

The ammeter (Fig. 6) monitors the current and is used for setting the current shut-off circuit at the proper level. By tests, it is found that the current gradually decreases from an initial maximum to less than half that value when tensile failure occurs. Then there is a discontinuity in current as it falls to less than a tenth of maximum. The gradual decrease is caused by a thinning of the wire which lessens the effective etching area. After breakage, the effective etch-area is drastically reduced, and causes discontinuity in current. We take advantage of this discontinuity to shut the current off. By means of a replay, a current shut-off circuit automatically shuts off the etching voltage when the current falls below about one-third of its initial or maximum value (Fig. 6 and Appendix).

Tungsten tips have been formed with various lengths extended below the surface. It was found that 2 mm of wire below the surface produces the best points. If there is more wire below, it becomes more expensive to use the $\langle 310 \rangle$ type. If there is less wire below, the lack of weight causes the breakage to occur too slowly and a smaller α and r are obtained. .The latter is to be avoided since there is a greater possibility of damage due to vibrations. It is important to keep the etching apparatus on a stable surface and prevent vibrations, especially near the crucial time of tensile failure. Slight movements of the surface have been found to give poor results. The results of various etches are catalogued in the results section (pp. 31 and 32).

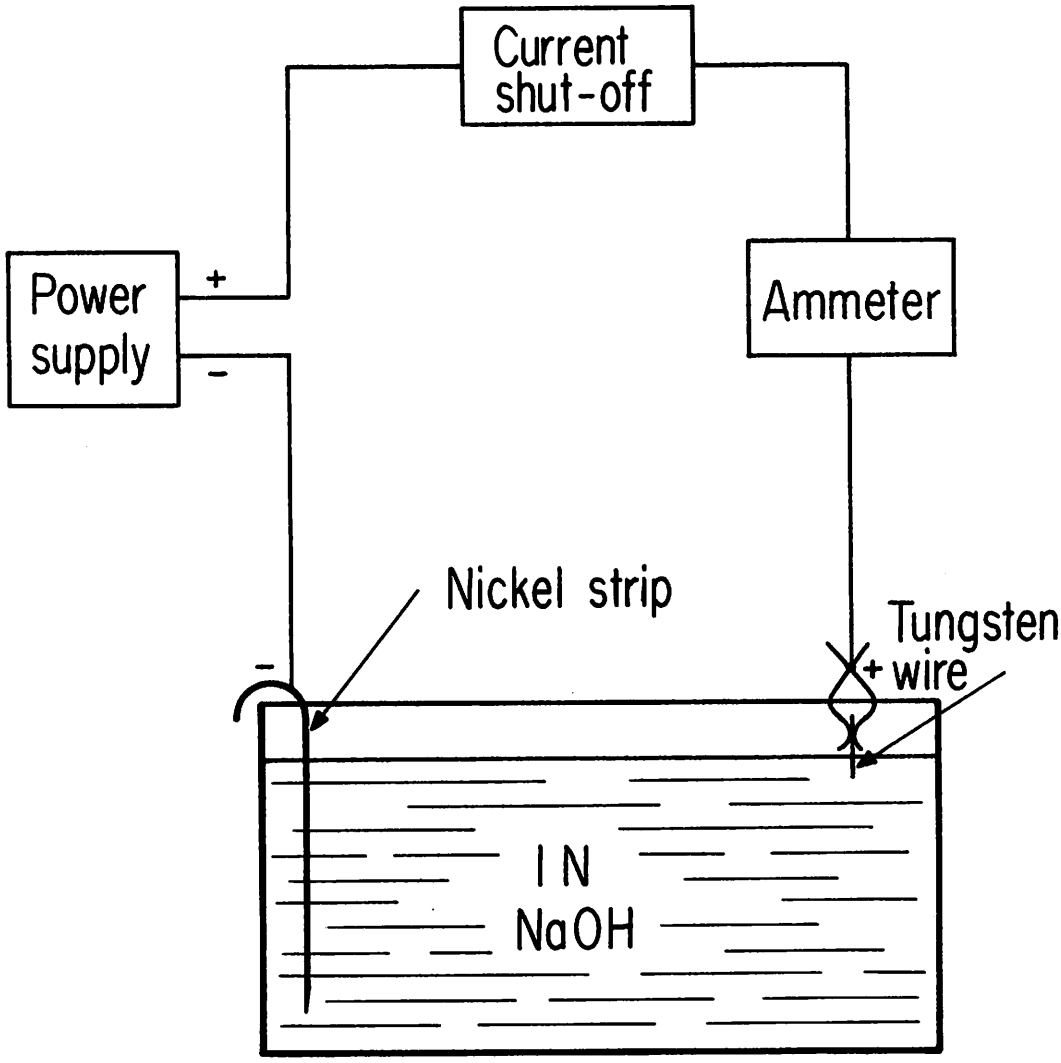

Fig. 6. The electrolytic etch apparatus

As mentioned above, the point of the tip will blunt if the current is not shut off soon after tensile failure. We take advantage of this phenomenon in an attempt to obtain our desired tip radius (r). The radius of the tip is often less than 3000 Å after the initial etch. This is too small for our purposes; a value between 4000 Å and 1 micron is more appropriate. By post-etching the tip for a specified time, the desired radius can be approached.

The apparatus used for post-etching consists of the same etching solution and power supply used in the initial etch. However, the voltage is supplied directly to a one-shot multivibrator (Appendix) which, in turn, supplies a pulse of 7 volts to the etching cell (Fig. 7). The time length of the pulse can be varied from 0.05 to 2 seconds and is monitored on an oscilloscope.

The usual procedure has been to remove the tip after the initial etch, examine it under an optical microscope, and record its apparent r and α. Then the tip is placed back in solution such that 1 mm or less extends beneath the surface. At these depths, there is no predominance of etching at the meniscus. If there was, the post-etch pulse time is so short that it would be negligible. The results show that pulse times between 0.2 and 2 seconds bring the radius within the desired range (Results, p. 29). The radius increases monotonically with pulse time; whereas, the cone half-angle (α) remains fairly independent of pulse time within the 0.2 - 1 second range.

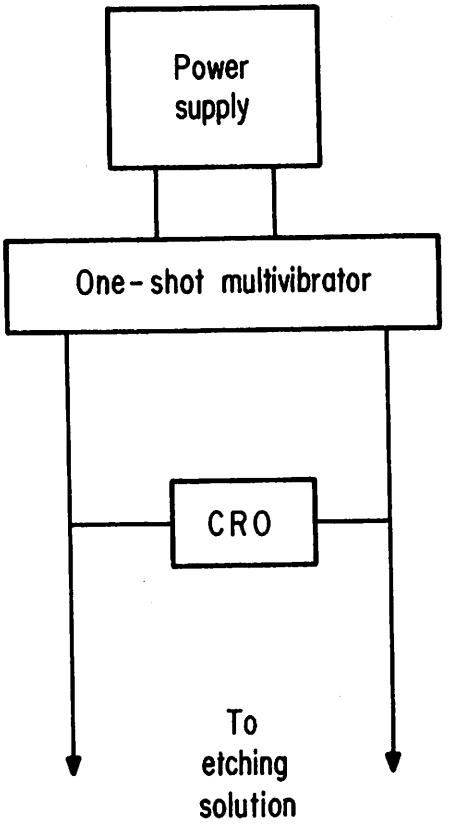

Fig. 7. Postetch circuit

The measurements of r and α are made with the aid of microscopes. As the most convenient method, an optical microscope is used together with a reticule built in the eyepiece. The tip is brought near the reticule image and an estimate is made of the radius. Since α is difficult to measure by this method and the visual estimate of r is not especially accurate, Polaroid photographs of some of the tips have been taken with a suitably equipped optical microscope. For these pictures, a phase interference apparatus, a 60-power objective, and a 20-power eyepiece are used. The time of exposure is set at 1 second while the light illuminates the tip from below. This bottom, or direct, illumination produces a shadow-image that has the property of showing a well-defined tip outline. With reflected or combined illumination, the true outline is not so evident. For a measurement of r, a picture has been taken of a ruled microscope slide with lines placed 10 microns apart.

Since the desired tip radii were near the resolution limit of the optical microscope (a few thousand angstroms), the resulting photographs contained pronounced diffraction patterns. Thus, a scanning electron microscope, with a resolution of a few hundred angstroms was used to calibrate the results of the optical microscope photographs. Once this was done, we need only use the much more convenient optical microscope. Results and comparisons of these estimates are given (Results, p. 37).

III. TEST APPARATUS FOR FIELD EMISSION TIPS

A. Anode Assembly

A high electric field must be impressed by placing a large potential voltage between the cathode tip and an anode. As can be seen from Eq. 7, the shape of the anode is not important but its distance (R) from the tip is. From considerations of secondary-electron emission, however, the shape becomes important (5, p. 11). Electrons are emitted from the tip and travel to the anode where they are collected. Some secondary electrons are created however; and if these are not eventually collected by the anode, the current will diminish. Further complications may result since the diminishment will probably be nonlinear with respect to the voltage. The more completely the anode surrounds the tip, the less possibility is there of electrons escaping.

Two different anodes were used with the emitter in the Kovar-glass base. The first one was made of semispherical shape formed by impressing a test tube against melted solder (Fig. 8). The semispherical anode was made to approximate closely the equipotential surfaces near the tip. Later it was realized that as long as the cathode-anode distance is very large compared with the tip radius, this is not necessary. Since the cathode-anode distance is chosen at about 5 mm and the tip radius never exceeds 1 micron, little regard was given to shape in design of the second anode.

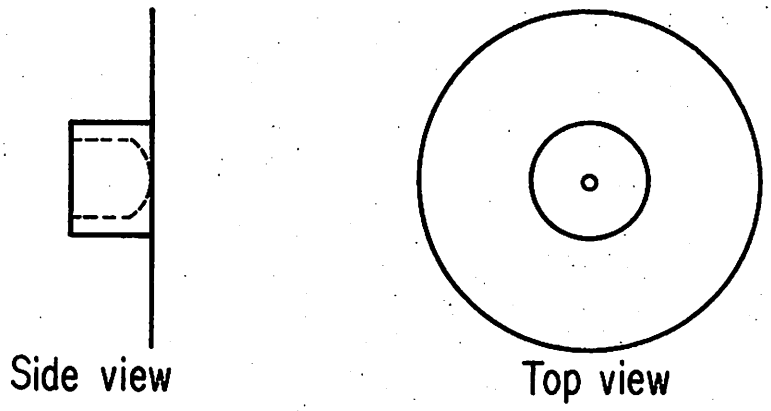

Fig. 8. Semispherical anode

The second anode was made to overcome some of the faults of the first. Those faults are: (1) the semispherical anode does not surround the tip enough to prevent loss of secondary electrons, and (2) the solder with which the anode is formed may not be the best anode material since it has a low thermal conductivity and low melting point. Thus the second anode was made of stainless steel in the shape of the frustrum of a cone. Due to the width of the Kovar-glass base, the cone frustrum was made such that one end has a diameter sufficient to clear it, while the other end has a diameter twice the cathode-anode distance (Fig. 9).

A Faraday cup is placed below the anode (Fig. 10). A 1-mm diameter hole was made in the anode to allow the electrons emitted in the forward direction to be collected by the Faraday cup. This is an important consideration for an electron source intended to be used in an electron microscope. A Faraday cup was used since it captures nearly all the electrons that come into its apperture, and has negligible secondary emission losses. The cup is placed about 4 mm from the anode.

B. The Initial Vacuum Assembly

The initial vacuum assembly is shown in Fig. 11. Three tubes containing insulated electrical connections hang down past the cathode on the vertical arm. The tubes serve as mechanical supports

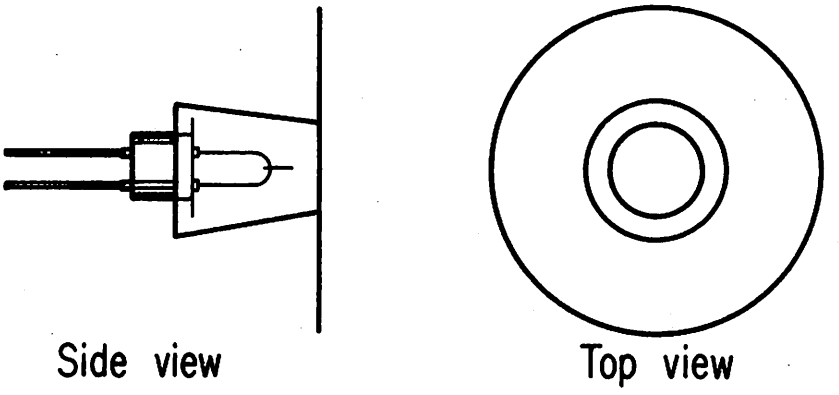

Fig. 9. Conical anode (containing the Kovar-glass base)

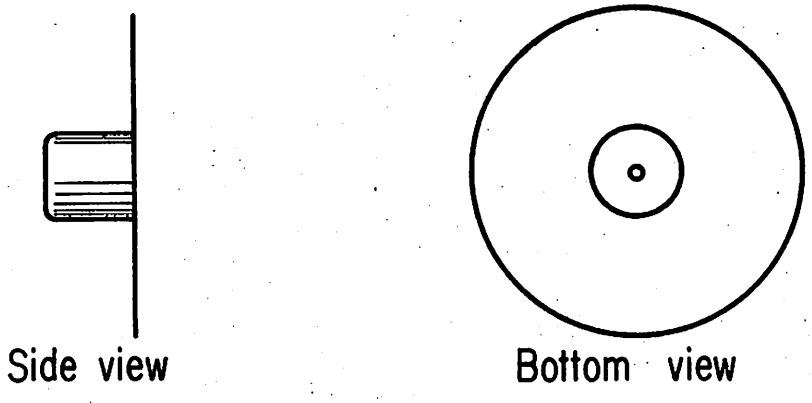

Fig. 10. Faraday cup

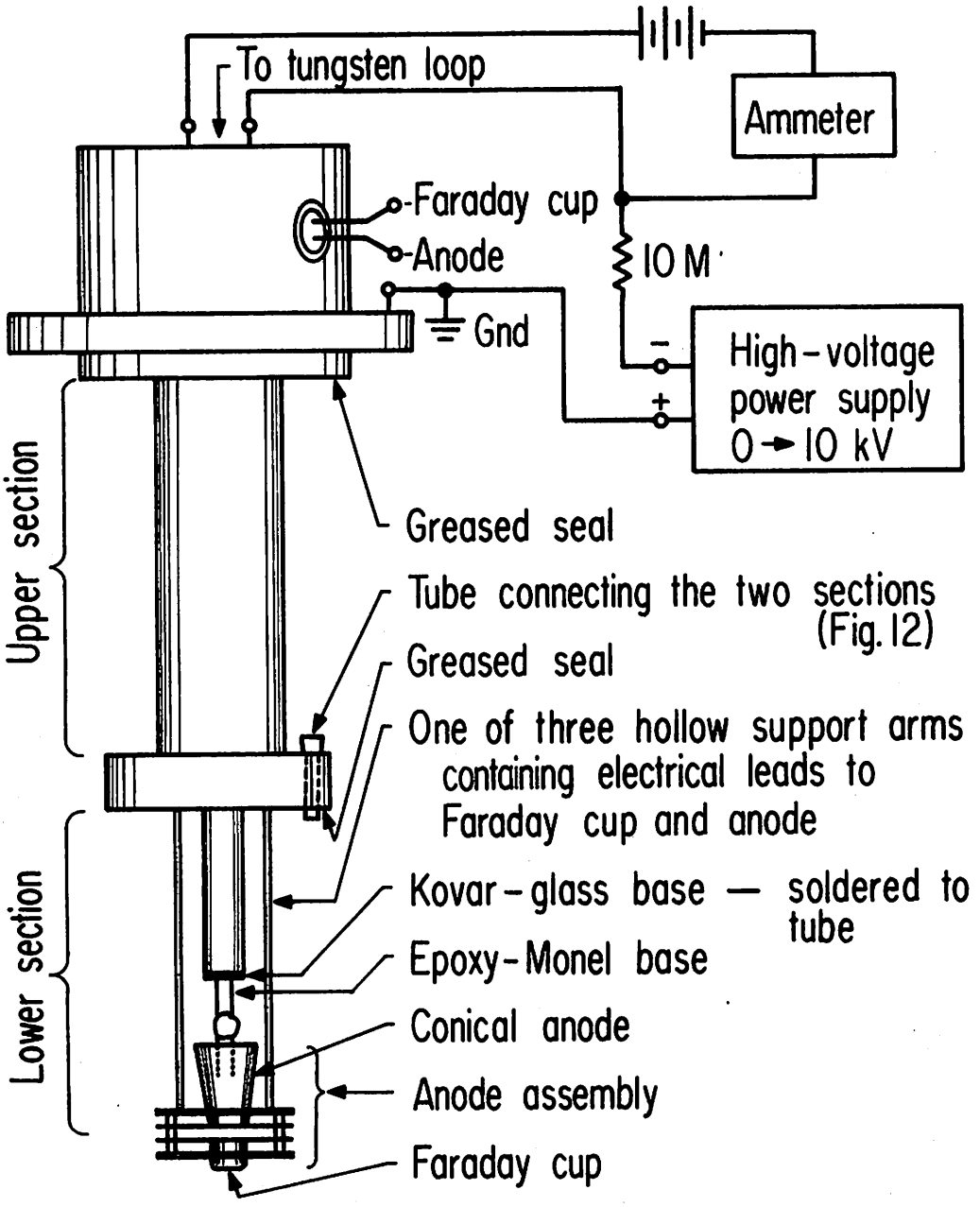

Fig. 11. The initial vacuum assembly

and electrical conduit for the anode and Faraday cup. The position of the anode assembly may be slightly altered on the supports providing a means of controlling the cathode-anode distance.

The vacuum chamber is evacuated by means of a standard pumping station containing a mechanical pump, a diffusion pump, and a cold trap. The lower section, which contains the emitter, can be sealed off from the upper. A narrow tube connects the two sections and allows the upper to be pumped down (Fig. 12). A small piece of vacuum grease is placed around the top of the tube end and, at the appropriate time, is heated such that it flows into the chamber. It thus separates the lower section from the upper.

To speed outgassing, the chamber and u-tube cold-trap are heated with a hot-air blower for about ten minutes. Then the vacuum chamber and u-tube are submerged into liquid nitrogen to the top of the lower section. Thus, the entire lower section is surrounded by an environment at liquid nitrogen temperature, ensuring a sufficient vacuum for our purposes.

C. Final Vacuum Assembly

Although the initial vacuum assembly allowed us to demonstrate field emission suitably stable for our scanning microscope, it gave only a crude idea of the directional properties of the emission.

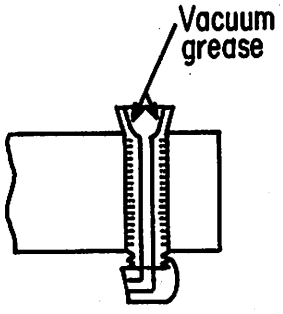

Fig. 12. Tube - connecting the two sections

Thus, after funds became available, it was decided to build a convenient test station with which we could view the emission pattern directly.

This system, first built by Savage and Low (6), is described below. It utilizes liquid helium to obtain a vacuum of $\sim 10^{-13}$ torr.

Figure 13 is a rough schematic diagram of the test station. A valved port (a) is utilized in initial evacuation. The liquid helium is contained in a chamber (b) which is supported by a stem (c) of low thermal conductivity. The stem also serves as the helium filling-tube and vent for escaping helium gas. A radiation shield (d) is supported by the stem at an intermediate point. The field emission tube (e) is attached to the bottom of the helium chamber so that its walls are cooled to near liquid helium temperatures. A high-voltage Kovar-glass fitting (f) is used for the cathode leads, while smaller Kovar-glass fittings (g) are used for the other leads.

The test station was initially built, as Savage and Low intended, for use as a field emission microscope. A fluorescent screen (h) and viewing window (i) would have then provided a display of the emission pattern. Since a suitable screen and window were not ready in time, alterations were made to accommodate our previously described anode assembly. The anode assembly was put in place of the fluorescent screen (h), and a plug put in place of the window (i).

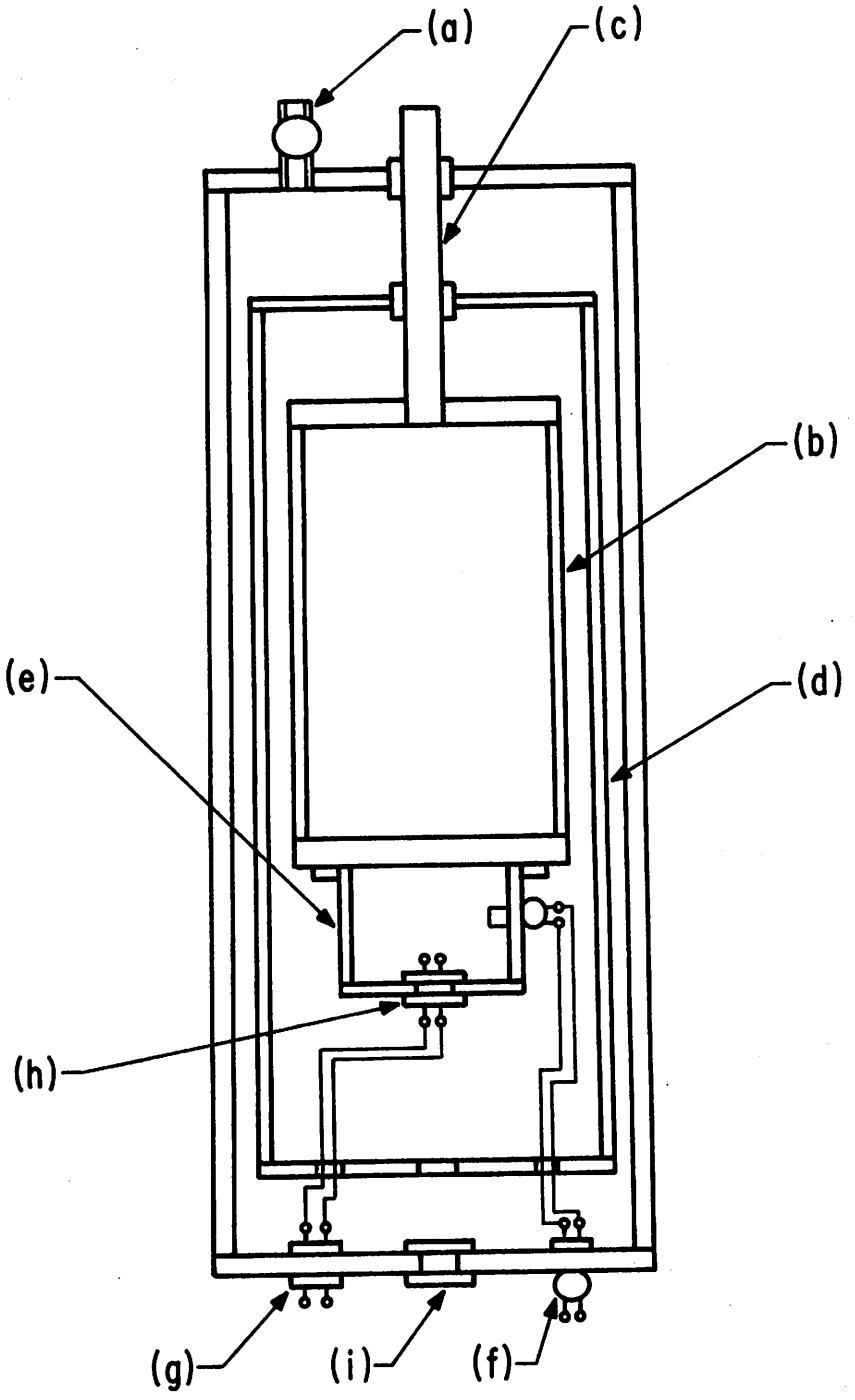

Fig. 13. The final vacuum assembly

A schematic diagram of the field emission tube, together with the alterations, is shown in Fig. 14. A j-shaped tube is included as a trap for gases migrating into the field emission tube.

IV. RESULTS

Tip Size

The results of etching the various tips are shown in Table 1. From this table, plots were made showing the average initial current versus the depth of the tip (Fig. 15), and the average time of etch versus the depth of the tip (Fig. 16). It can be seen (Fig. 15) that the average initial current increases with the length of wire in solution. Some of the scatter in the data might be due to an orientation dependence of the etching speed.

Table 2 gives the results of post-etching the tips. The tip radius (r) given in this table is measured by two means, both of which utilize an optical microscope. One is an eye-estimate and the other is an estimate made from a photograph. These estimates are plotted versus pulse time in Fig. 17. As can be seen, there is considerable variation. However, when averages are taken at common pulse lengths, a monotonic relationship results. That is, the radius of the tip appears to increase with pulse length. We also notice that the photo-estimate looks on the average to be a little larger than the eye-estimate. By extrapolation, to obtain a tip with $r = 0.7\mu$, we would post-etch it for about 1.4 seconds.

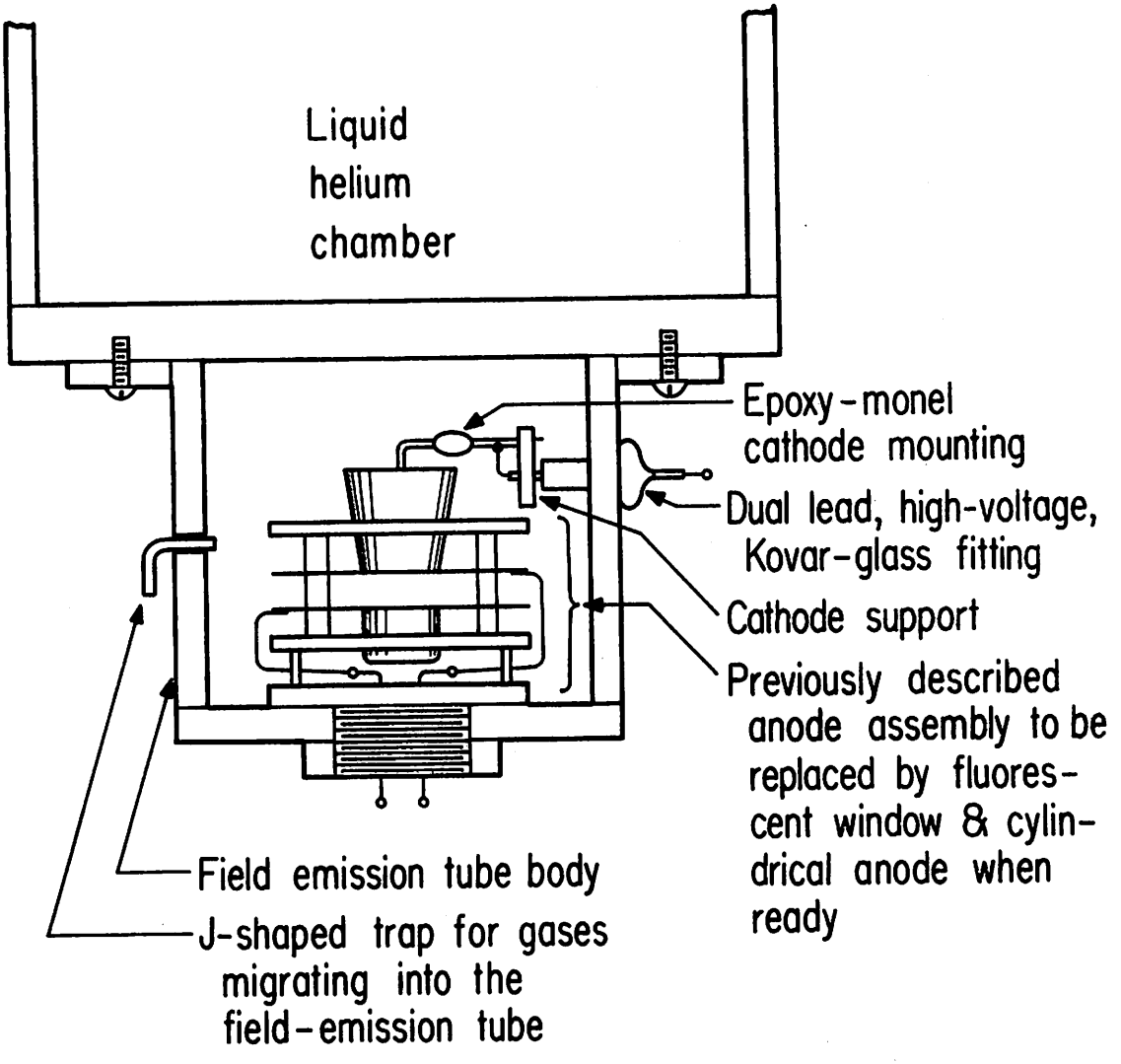

Fig. 14. The field-emission tube - with alterations

Table 1. Etching of Tips

Tip	Radius (mil)	Depth (mm)	Initial Current (ma)	Time (sec)
A_1	6	1	1.4	370
A_1	6	3	2.8	420
A_2	6	2.5	3.2	485
A_3	6	3	3.8	540
A_4	6	1.5	2.5	563
A_5	6		48	375
A_8	4		18	393
A_{11}	4		5	360
A_{12}	4		13	390
B_1	4	-	7.3	968
B_2	4	-	6	600
B_3	4	-	6.9	593
B_4	4	-	8.2	590
C_1	4	3.5	4.4	499
C_2	4	4.5	5.3	455
D_1	4	2.5	4.4	370
D_2	4	2.7	5.6	385
D_3	4	3	6.5	415
D_4	4	3	6.4	420
D_5	4	3	5.8	395
E_2	4	3	4.6	300
E_6	4	3	5.7	255
F_1	4	3	5.3	~300
F_2	4	3	5.5	405
F_3	4	2.5	5.5	320
G_2	5	3	3.9	630
G_3	5	2.7	3.7	673
H_1	5	1	1.7	615
H_2	5	2	3.4	634
H_3	5	2	3.8	631
H_4	5	2.5	4.8	612

Table 1 (Cont'd.). Etching of Tips

Tip	Radius (mil)	Depth (mm)	Initial Current (ma)	Time (sec)
I_1	5	2.2	3.1	646
I_2	5	2.4	2.7	686
I_3	5	2.6	3.6	721
J_1	5	2.5	4	555
J_2	5	2.1	3.7	651
J_3	5	2	3.4	656
J_4	5	2	3.4	663
J_5	5	2	3.9	683
J_6	5	2	3.8	669
J_7	5	2	3.4	673
J_9	5	2	3.7	728
J_{10}	5	2.2	3.4	720
K_1	5	2	3	754
K_2	5	1.9	2.5	750
K_3	5	2	2.8	728
L_1	4	1.9	2.7	490
L_2	4	2.1	3.1	423
M_1	5	2	3	915
M_2	5	2	2.8	788
M_3	5	2	3.4	620
M_4	5	2	3.5	560
M_5	5	2	3.6	560
M_6	5	2.2	3.3	650
M_7	5	2	3.7	602
N_1	5	2	3.4	625
0_1	5	2.2	4.3	470
0_2	5	2	4.1	$\langle$600
P_1	5	2	3.4	-
P_2	5	2	4.4	615
P_3	5	2.1	3.5	$\langle$600
P_4	5	2.5	2.5	605

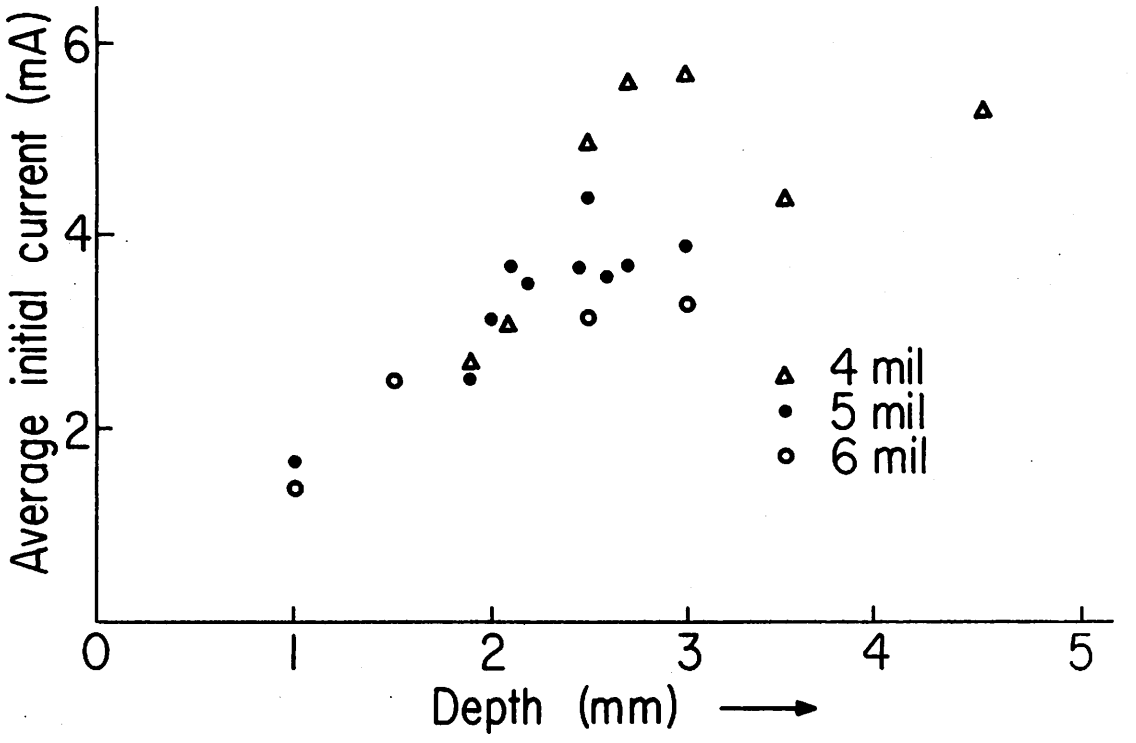

Fig. 15. Tip etching - Average initial current vs. tip depth

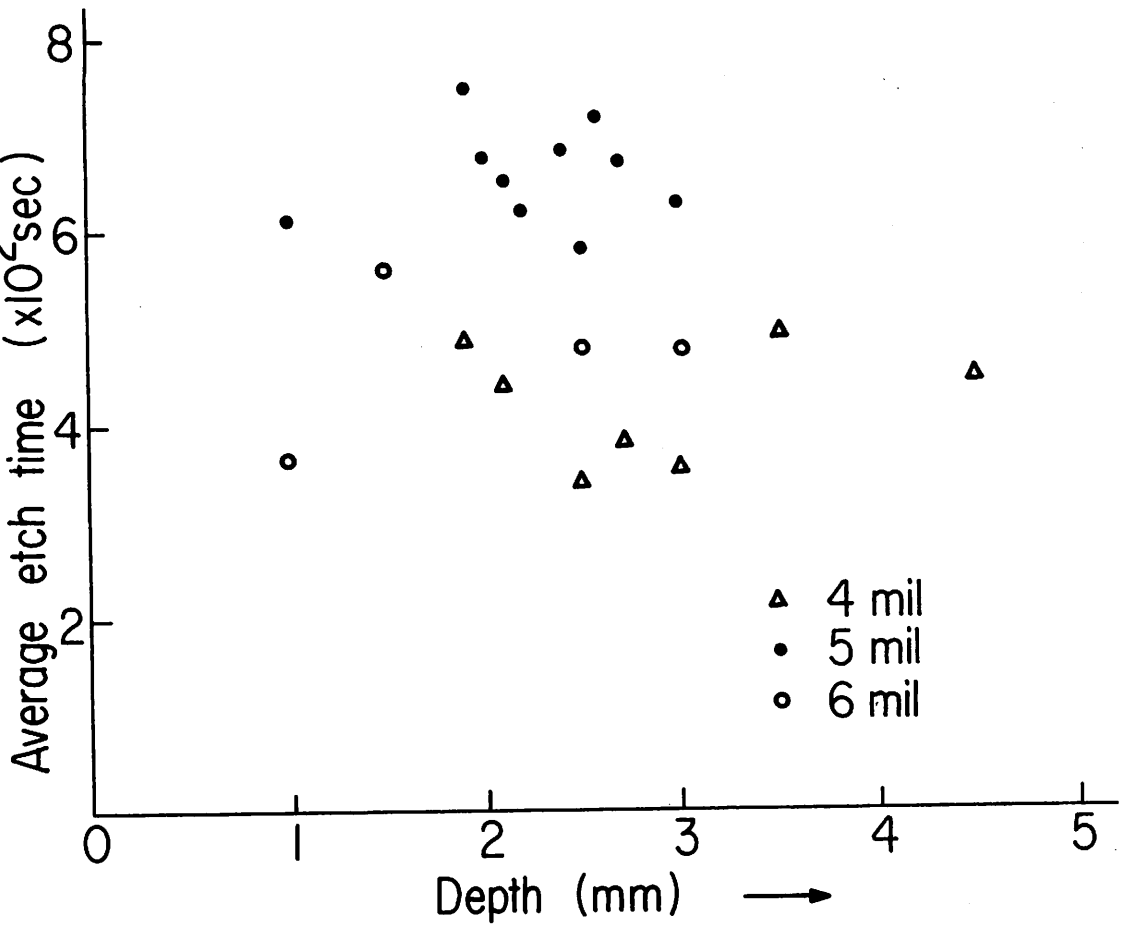

Fig. 16. Tip etching - Average etch time vs. tip depth

Table 2. Post-etching of Tips

Tip	Pulse length (sec)	Eye-estimate Tip radius (Å)	Photo-estimate Tip radius (Å)
H_2	~1	5000	--
H_4	~1	5000	6300
I_1	~1	3000	2500
I_2	~1/3	<2000	--
I_2	~1	5000	7000
J_1	1	4000	--
J_2	0.8	4000	6300
J_3	0.2	<2000	--
J_3	0.4	2000	--
J_3	0.6	3000	--
J_3	0.8	3500	4500
J_4	0.4	2500	--
J_5	0.4	2000	4900
J_8	0.6	4000	8900
J_9	0.8	5000	--
J_{10}	1	9800	9800
K_1	1.08	1μ	--
K_2	1	4500	4400
K_3	1	4000	3700
L_1	0.9	2000	3650
L_2	~1	7000	5000
M_3	0.4	2000	--
M_5	0.4	8000	--
M_6	0.2	3500	--
M_7	0.4	4000	3650
N_1	0.8	6000	--
O_1	0.8	7000	7000
O_2	0.8	4000	4000
P_1	1.5	1.2μ	1μ
P_2	1.4	5000	5920
P_3	2	7500	8640
P_4	3.6	6000	3740

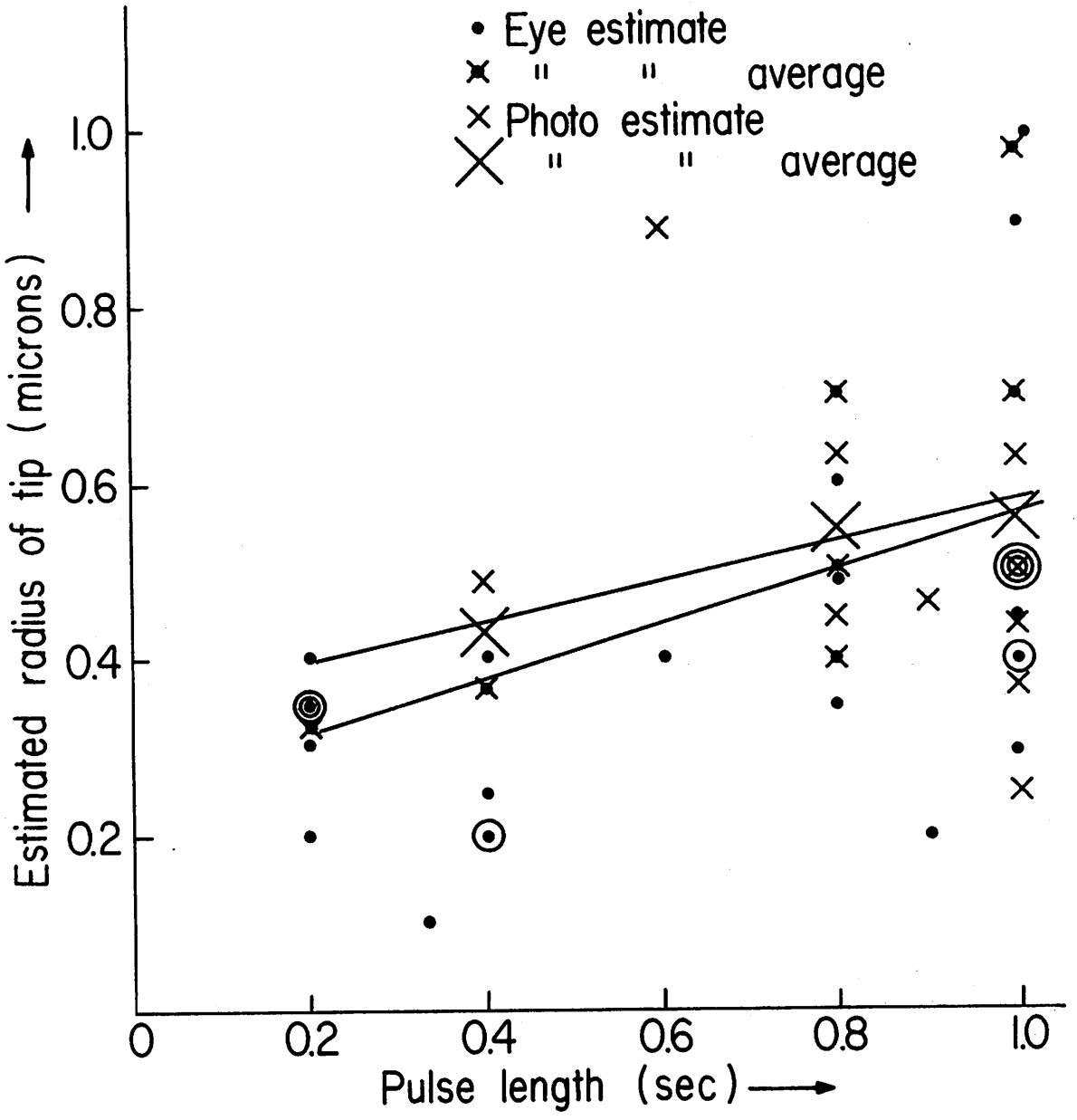

Fig. 17. Radius of tip as a function of pulse length

To see more accurately the relationship between each form of tip radius estimate, a plot was made showing the photo-estimate versus the eye-estimate of various tips (Fig. 18). If these estimates were in agreement, the points would lie on the 45^{o} line of Fig. 18. However, in agreement with Fig. 17, the photo-estimate appear to be, in general, larger than the eye-estimates. Considerable variation is also apparent in the plot of Fig. 18.

As a check on the accuracy of the optical microscope photographs, some tips were also photographed in a scanning electron microscope (SEM). Both optical and SEM photographs of two of these tips are shown in Figs. 19 and 20. Tip P_3 is better than Tip P_1. Measurements of tip radius (r) were made from these photos, and are plotted in Fig. 21. The optical microscope measurements appear to be roughly twice as large as the SEM measurements. This is probably due, in part, to diffraction effects associated with optical microscopy. Despite the variation, the relationship is monotonic and useful in obtaining the correct tip size. Half-angles of various tips are shown in Table 3.

Electrical Tests

We shall now describe four tests of current versus voltage under various conditions. The pressure was measured with a thermocouple vacuum gauge, and for each test it was better than 10^{-3} torr.

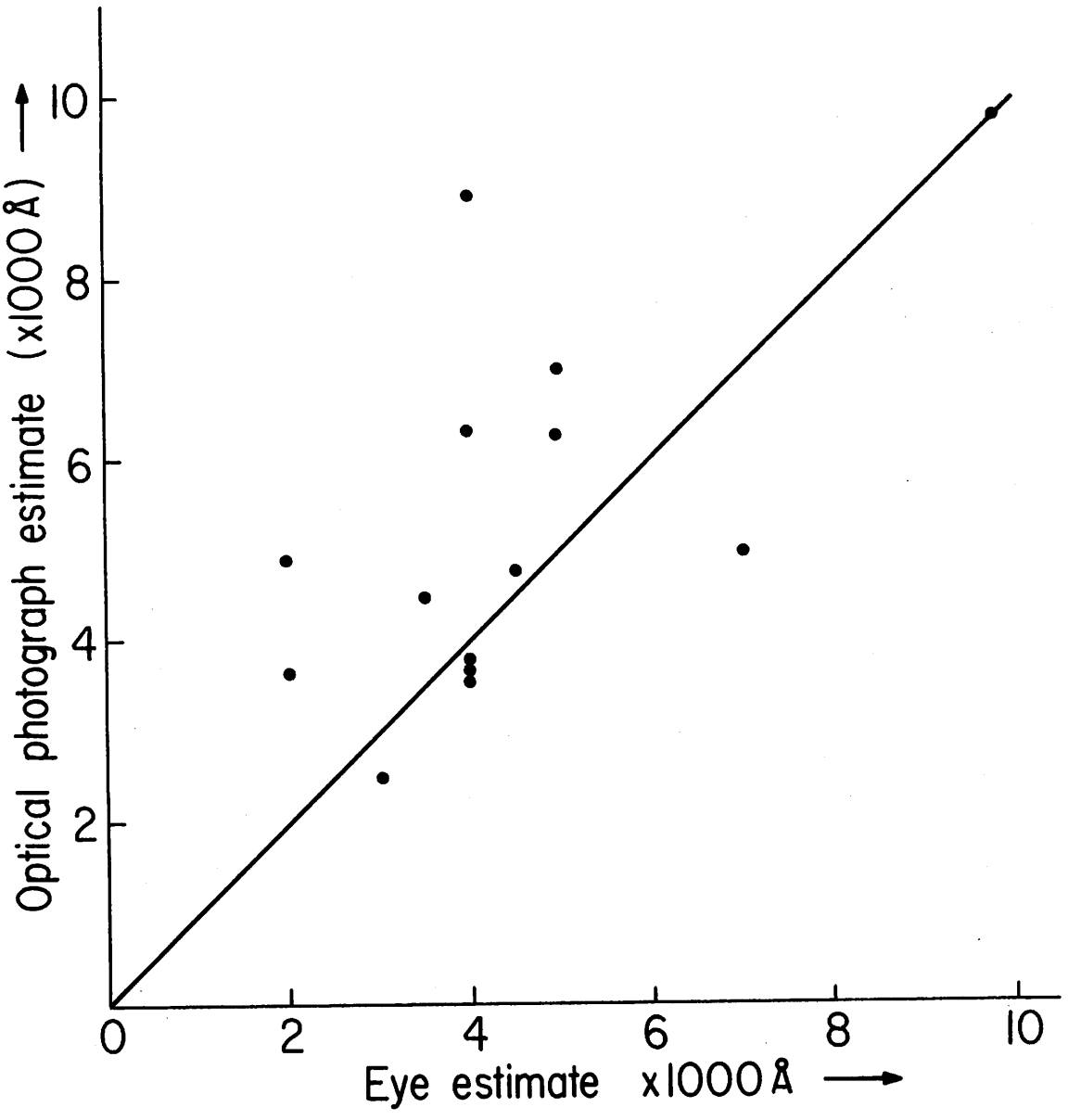

Fig. 18. Radii of various tips by optical methods

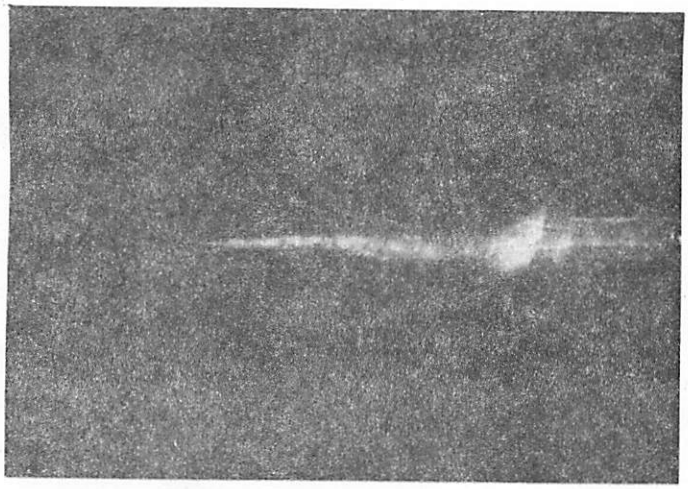

(a) SEM photo, 5 mil wire

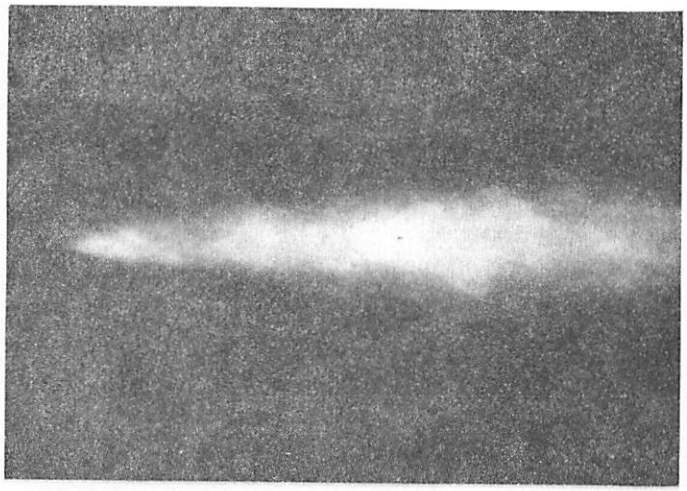

(b) SEM photo, 25x magnification of (a), 1mm = 3450 Å

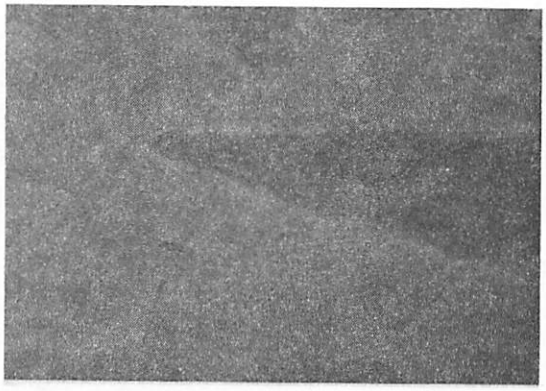

(c) Optical microscope photo, 1 mm = 9100 Å

Fig. 19. Comparative photos of Tip P_1

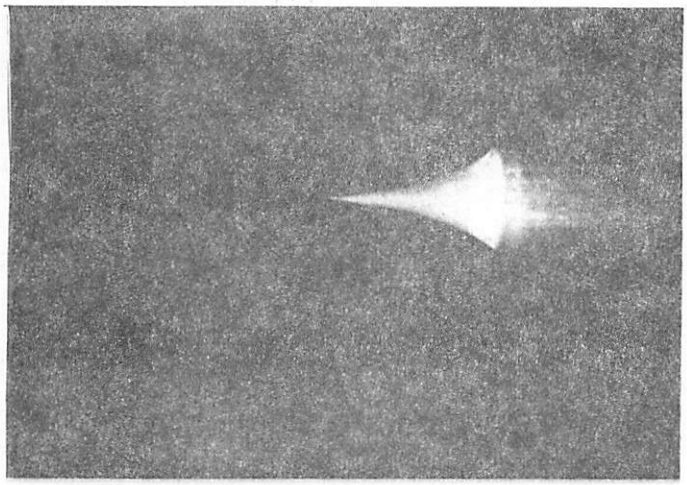

(a) SEM photo, 5 mil wire

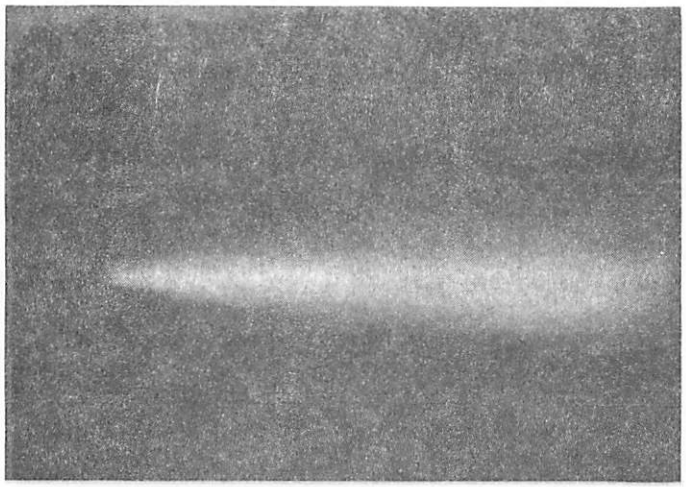

(b) SEM photo, 25 x magnification of (a), 1mm = 3450 Å

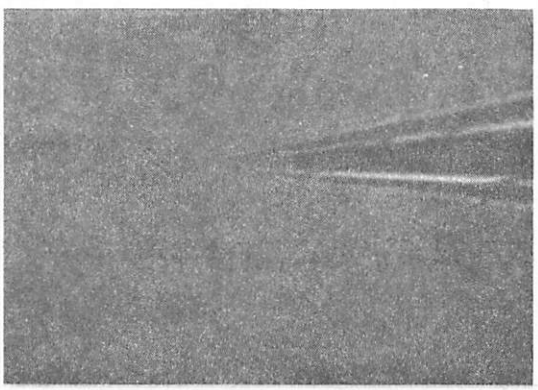

(c) Optical microscope photo, 1 mm = 9100 Å

Fig. 20. Comparative photos of P_3

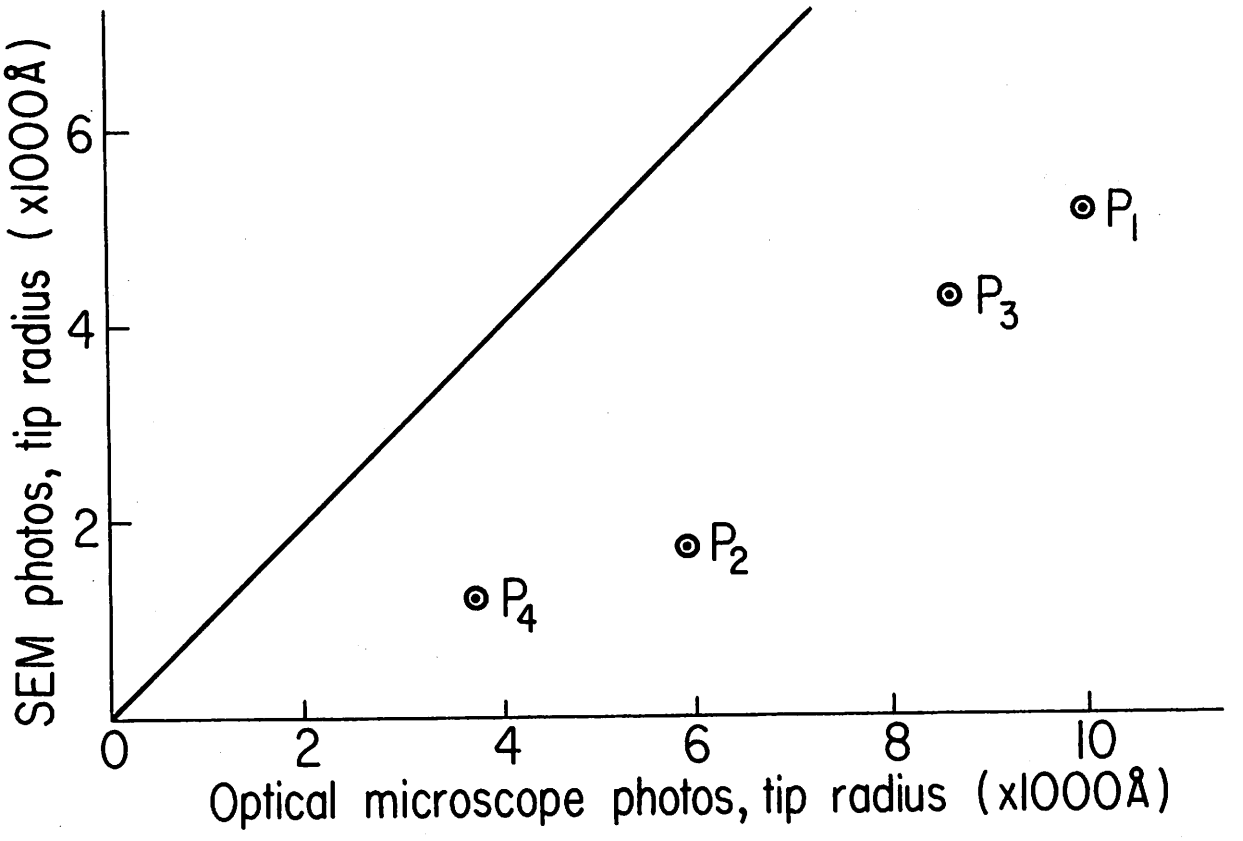

Fig. 21. Comparison of optical microscope and SEM photos

Table 3. Tip Half-Angles (Fig. 1), From Optical Microscope Photographs

Tip	Half-angle (α) (degrees)
H_2	8
H_3	3
H_4	7.5
I_1	8.5
I_2	7.5
J_2	6.5
J_3	6
J_5	7
J_8	7
J_9	3.5
J_{10}	7
K_{2L}	6
K_{2R}	6
K_{3L}	6
K_{3R}	5.5
L_1	8.5
L_2	9.5
M_3	6
M_6	5
M_7	4.5
N_1	8.5
O_1	16
O_2	10.5
P_1	8.5
P_2	7.5
P_3	8
P_4	7

Since a more accurate gauge was not used, we do not know just how much better than 10^{-3} torr the vacuum was for each particular run. Estimates from current versus time measurements, as discussed earlier (p. 5), were made and are noted on page 62.

The first test will be denoted as Run 1. The results are shown in Fig. 22. For this test, we used Tip F_3 in the initial vacuum system. From the cathode heating current and charts of temperature versus current (2, p. 16), the initial temperature was found to be approximately $600^{\circ}K$. The heating current was then increased in three steps. The results of these procedures (Fig. 22) show that heating causes a shift to the left of the I vs 1/V plot. That is, it takes more voltage to obtain the same current. This is believed to be due to blunting of the tip caused by heating at low fields (4, p. 23).

In the region below 200 mμamp, the Faraday cup data is linear as expected (Eq. 6), and is below the anode current. Above 200 mμamp, the anode current falls below the Faraday cup current. Because of the greater area of the anode, it would seem peculiar that the anode current should fall below the Faraday cup current. This, however, is probably caused by anode current losses due to secondary-emission. Since, for this run only, the anode was semispherical (Fig. 8) with a high potential for secondary-emission losses and the Faraday cup has negligible secondary-emission losses, this explanation appears plausible.

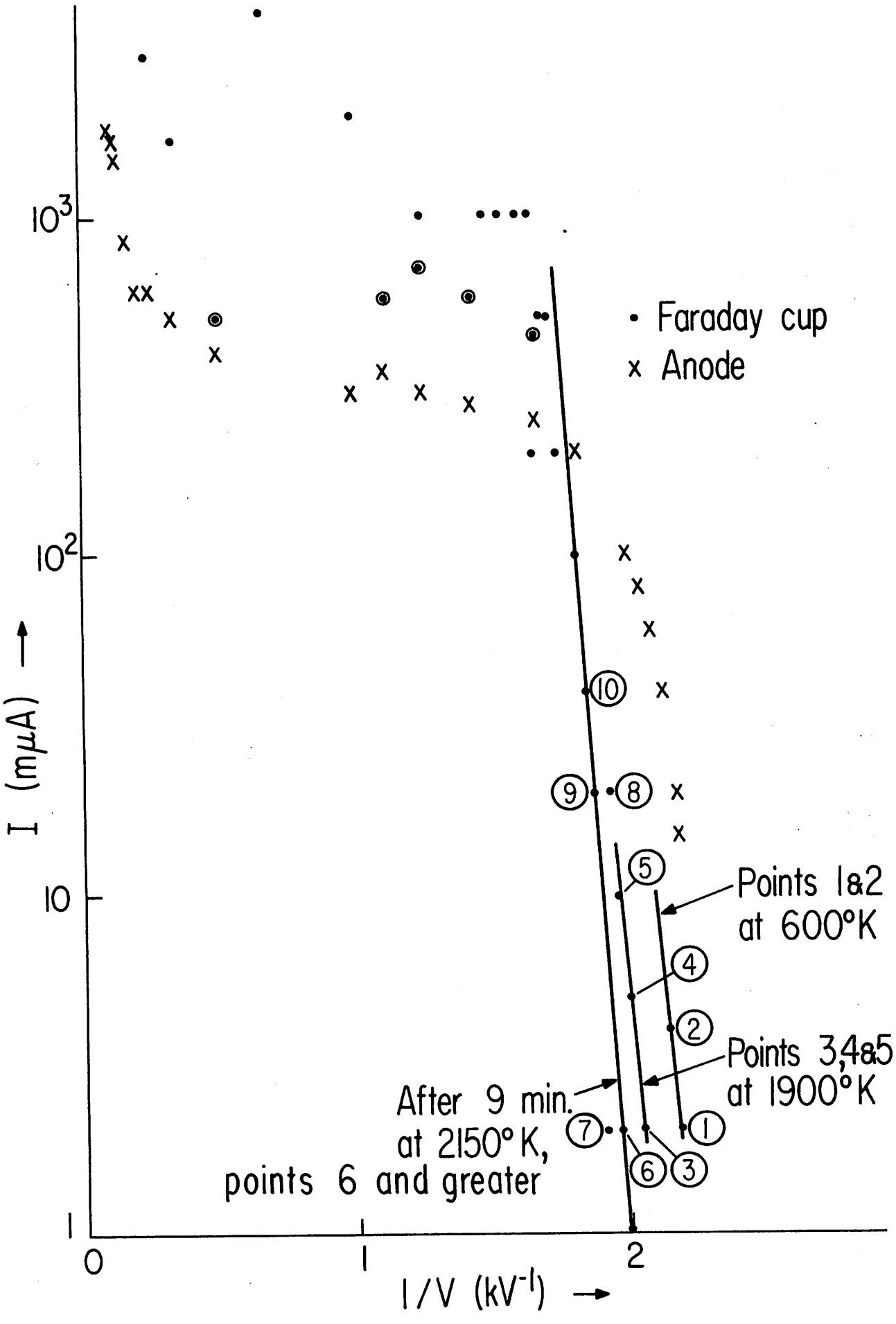

Fig. 22. Run 1 (Tip F_3)

Also, above 200 mμamp, the Faraday cup current was measured with both increasing and decreasing voltages. For decreasing voltage, the Faraday cup current fell below that for increasing voltage. This is believed to be due to ion bombardment of the tip at high currents causing tip blunting and a subsequent decrease in current.

Finally, the vacuum achieved in this test (Fig. 22) is not as high as would be desired since the initial vacuum system was used. This accounts, in general, for the irregular behavior in the region of high current density. In our most recent test with the new vacuum system, regular behavior at these currents was achieved.

Run 2 was made using the same tip and vacuum assembly (Fig. 23). The only difference was that no liquid nitrogen was added to improve the vacuum. Some linear behavior is apparent in the plot, although it becomes irregular at a much lower voltage and current ($V = 400$ volts, $I \cong 20$ mμamp) than in Fig. 22 where the vacuum was better. In general, the currents are lower by at least a factor of 10. The anode current is about 4 times the Faraday cup current. This is consistent with our hypothesis that ion bombardment in a poor vacuum causes dulling of the tip.

When the final vacuum system was ready, Tip O_1 was tested in Run 3. Since liquid nitrogen was used in the liquid helium chamber, the vacuum obtained was not optimum. Compared with the initial

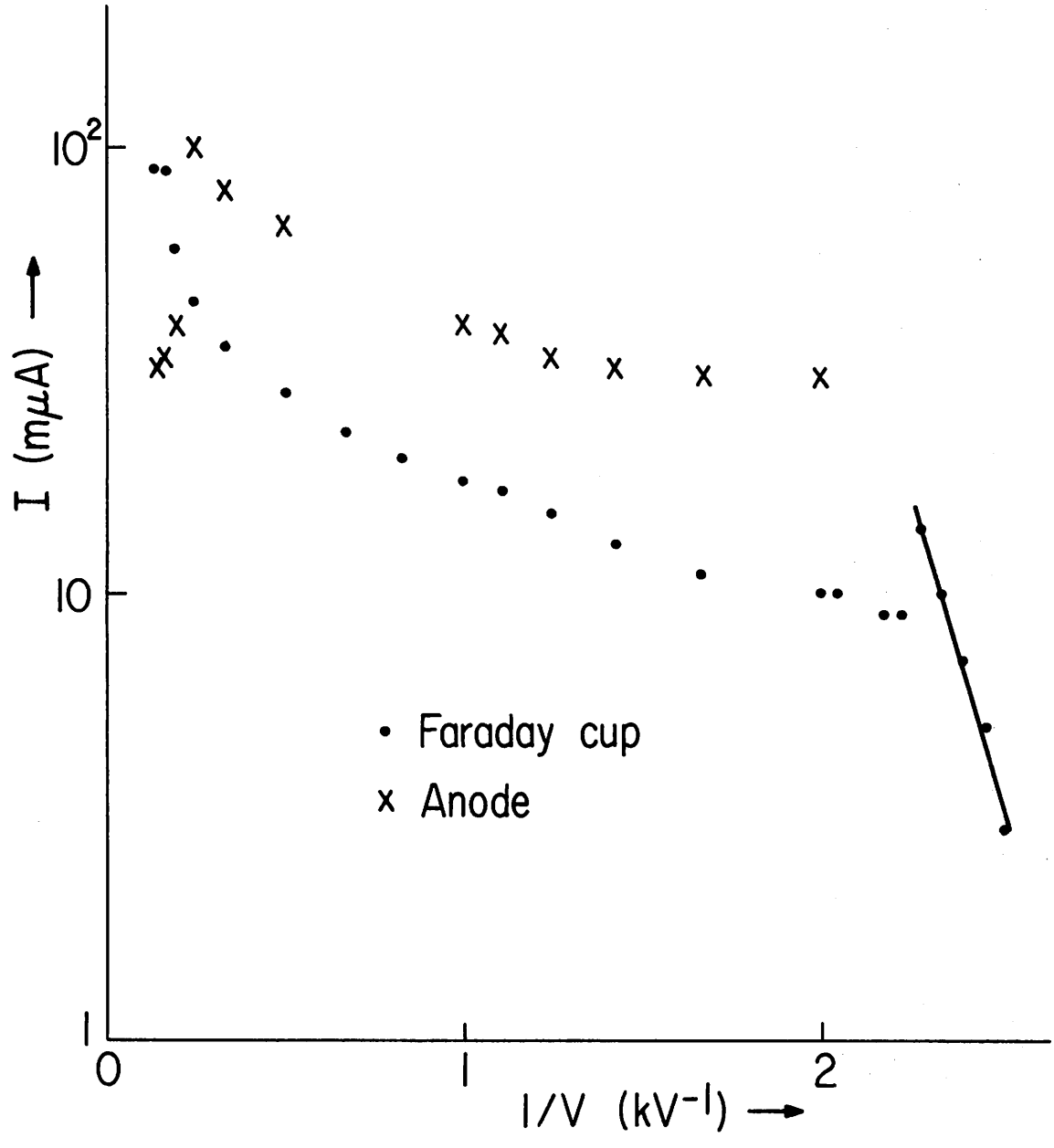

Fig. 23. Run 2 (Tip F_3, no liquid nitrogen)

vacuum assembly, however, it was an improvement. The heating current was such as to keep the tip at $\cong 250^{\circ}K$. The Faraday cup current was immeasureable (less than 10^{-12} amp). This is believed to have been caused by misalignment of the tip. The results are shown in Fig. 24.

In agreement with Eq. 6, the plots of Fig. 24 exhibit good linearity. There is disagreement with theory in that the results are not reproducible. That is, ideally there should be but one line not three or four shifted to the left by different amounts. The shifting of Test (a) is believed to have been caused by arcing at some point or points other than the cathode-anode assembly. This 'exterior' arcing would have the effect of reducing the cathode-anode voltage (V). The explanation appears plausible since the anode current was eventually impossible to measure. This could be explained by shorting. Also, at low V, as V was increased, the plot first shifts to the left then back again, which is typical of a temporary arcing.

Theoretical plots are shown with both Runs 3 and 4. The calculations leading to these plots are given in a separate section (Calculations, p. 61).

The difference in slope and the large shift to the left between Tests (a) and (b) (taken shortly after Test (a)) indicate a change in the tip radius (r), the work function (ϕ_e), or both. From Eq. 5 we see

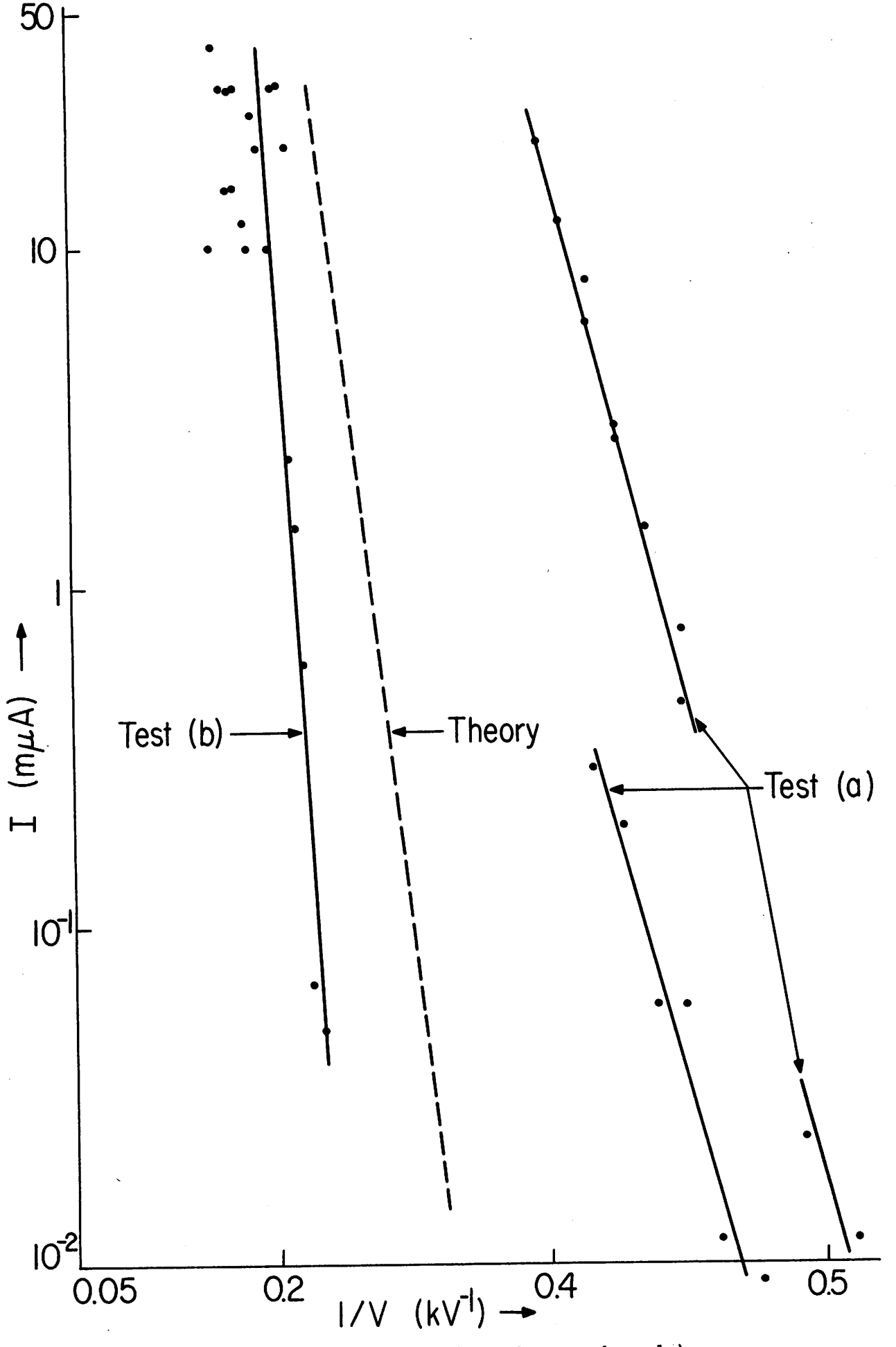

Fig. 24. Run 3 (Tip 0_1, anode only)

that an increase in work function would cause both a shift to the left and a decrease in slope. Such an increase could be caused by adsorbed gases. From Eq. 17 (Calculations, p. 60) we see that an increase in radius would cause a slight shift to the right and a decrease in slope. It is most probable, therefore, that the observed changes are caused by an increase in work function (1, p. 117).

Tip O_2 was tested in Run 4 in the final vacuum system. Liquid nitrogen was again used as the cooling agent. The temperature of the tip was kept at $\cong 225^{\circ}K$ while data were recorded. To prevent a negative charge from building up on the anode while the Faraday cup current was being measured, the anode was grounded for this measurement. Three successive tests were made which, henceforth, will be denoted as Tests 1, 2, and 3. Between Tests 1 and 2 there was a pause of about three minutes. Between Tests 2 and 3, with V = 2 kV, the tip temperature was increased to $\cong 1430^{\circ}K$ for about one minute.

Figure 25 shows the results of Test 1. The Faraday cup current is at least a factor of 10 less than the anode current.

In Fig. 26, the results of Test 2 are shown. Here, the Faraday cup current is about a factor of 2 less than the anode current. A comparison of the results of Tests 1 and 2 shows that the slope of Test 2 is greater than that of Test 1. This increase in slope may have been caused by a decrease in radius (r) or a decrease in work function (ϕ).

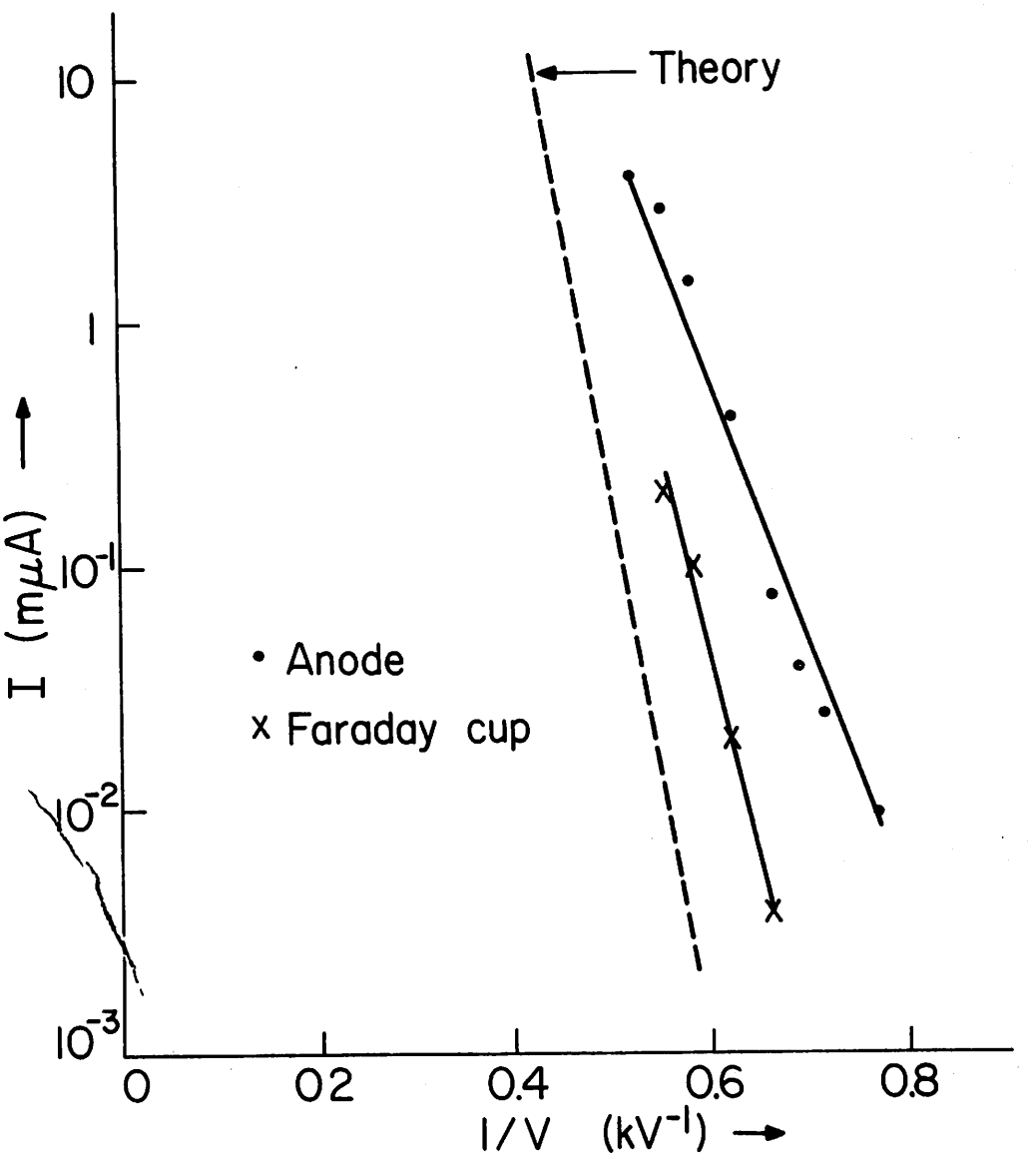

Fig. 25. Run 4, test 1 (Tip 0_2)

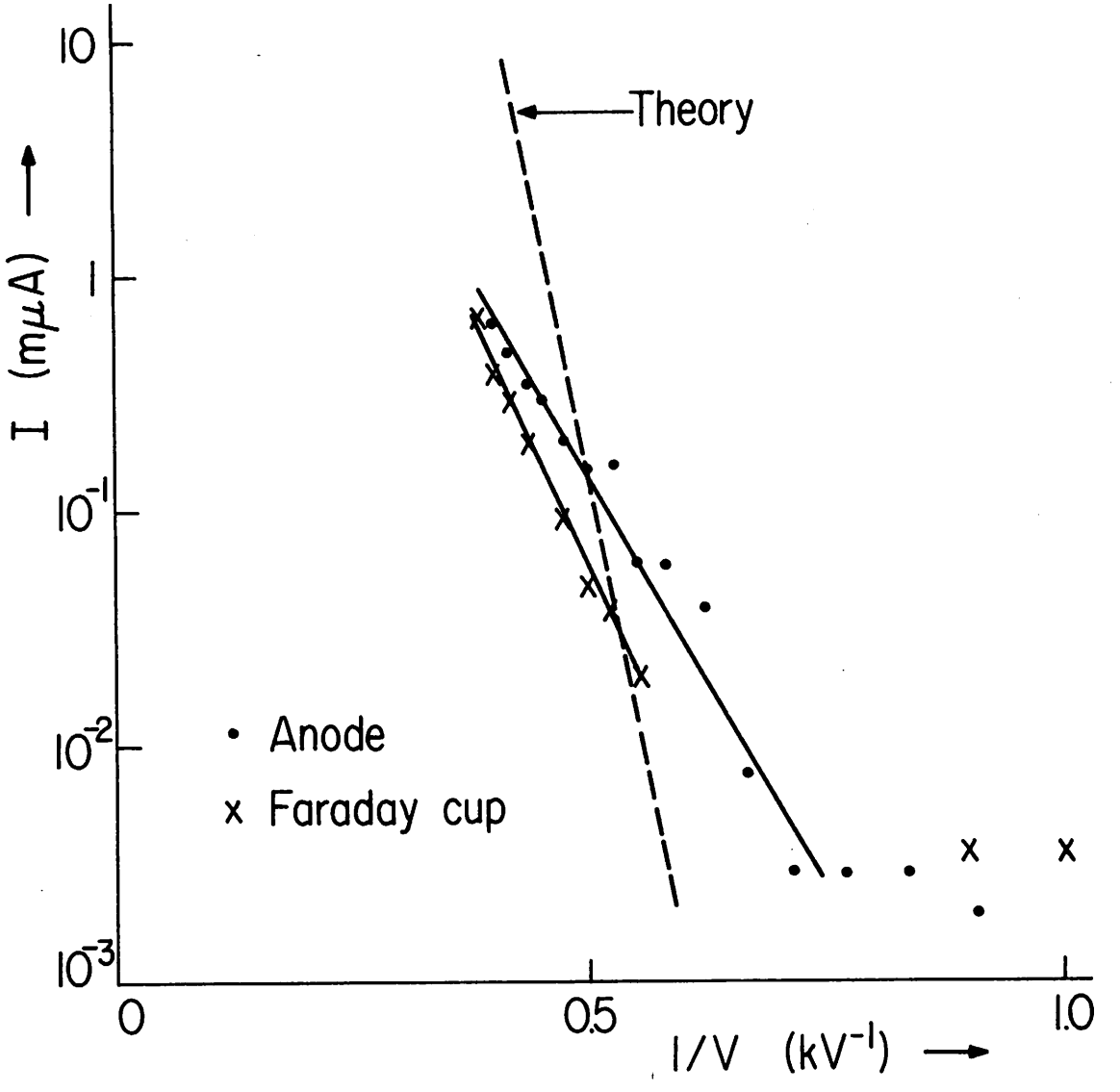

Fig. 26. Run 4, test 2 (Tip 0_2)

A decrease in r might have come about by surface migration of tungsten in the tip (1, p. 153). This however is unlikely since the tip temperature of $\cong 225^{\circ}K$ is too low for surface migration to occur. A decrease in ϕ is more probable. The greater proportion of electrons reaching the Faraday cup in Test 2 suggests a change in the emission pattern. This also supports the change in work function hypothesis.

Figure 27 shows the results of Test 3. The Faraday cup current is a factor of 1000 smaller than the anode current. A comparison of the results of Tests 2 and 3 shows that the slope of Test 3 is less than that of Test 2. An increase in ϕ_e is believed to have caused the slope decrease (Eq. 5). Such an increase in ϕ was probably caused by extrusion of the tip (5, p. 6). This would have been caused by the $1430^{\circ}K$ heating at a high voltage immediately preceding Test 3. A change in work function could have also contributed somewhat. The idea of tip extrusion as being the main factor in the slope decrease is supported by evidence that a much smaller proportion of the electrons reach the Faraday cup in Test 3 than in either of the preceding tests. To illustrate this, Fig. 28 shows a typically extruded tip (7, p. 795) and its probable emission pattern. As can be seen, the fraction of electrons emitted in the forward direction is decreased after tip extrusion. Test 3 also shows that currents up to 1μamp can be reached with good linearity. In general, all three tests show, by their linearity, good agreement with Eq. 6.

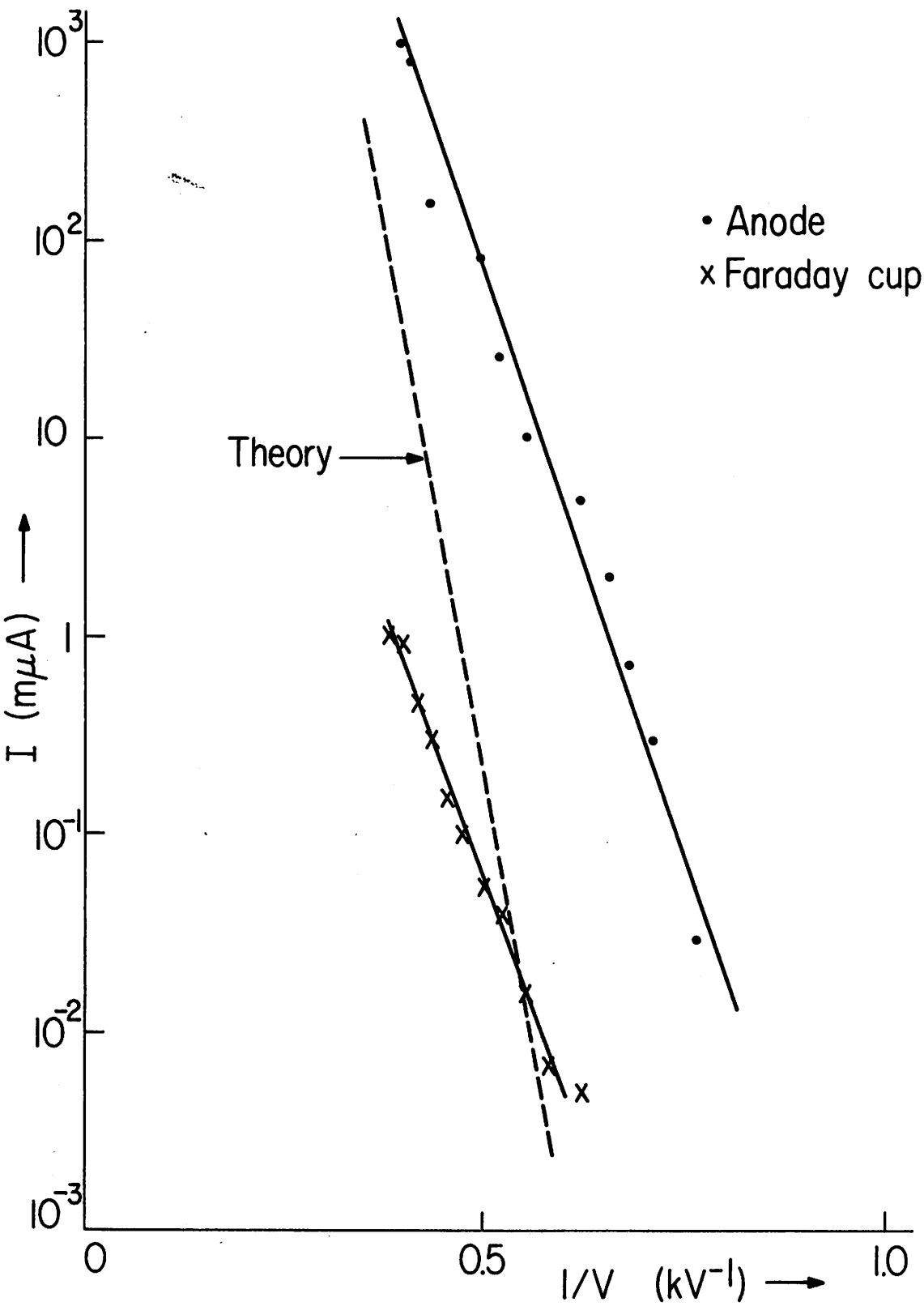

Fig. 27. Run 4, test 3 (Tip 0_2)

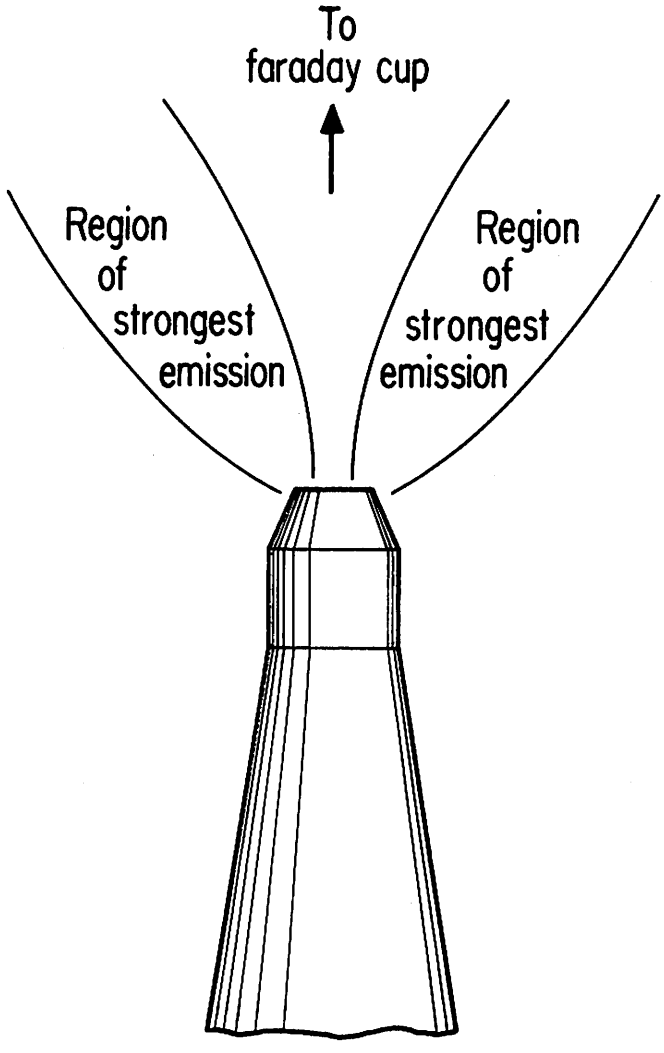

Fig. 28. Extruded tip and probable regions of strongest emission

With the voltage at 3 kV, a current-time test was made after Run 1. Figure 29 shows the results of this test. It may be observed that the current is fairly stable for about ten minutes. From this we estimate (Calculations, p. 62) that the vacuum was better than 10^{-7} torr.

Another current-time test was made after Run 2 with conditions identical to those in the previous test except for the absence of liquid nitrogen to bring the vacuum below 10^{-3} torr. The results of this test are shown in Fig. 30. There is an observable decay from which an estimate of the pressure can be made (Calculations, p. 63). This estimate is a factor of about 100 less than the 10^{-3} torr measured on the thermocouple vacuum gauge during Run 2.

For about two minutes of this test, the tip was heated to $\sim 1430^{\circ}$K. The immediate results of this increase in temperature can be seen as an increase in current (Fig. 30). This is an illustration of T-F emission. The after effects of the temporary temperature increase produce a slight rejuvenation of the tip. That is, when the temperature is brought down to $\cong 300^{\circ}$K again, the current level is higher than it was immediately before the temperature increase. It is believed that the higher temperature has the effect of restoring the tip by driving off residual gases.

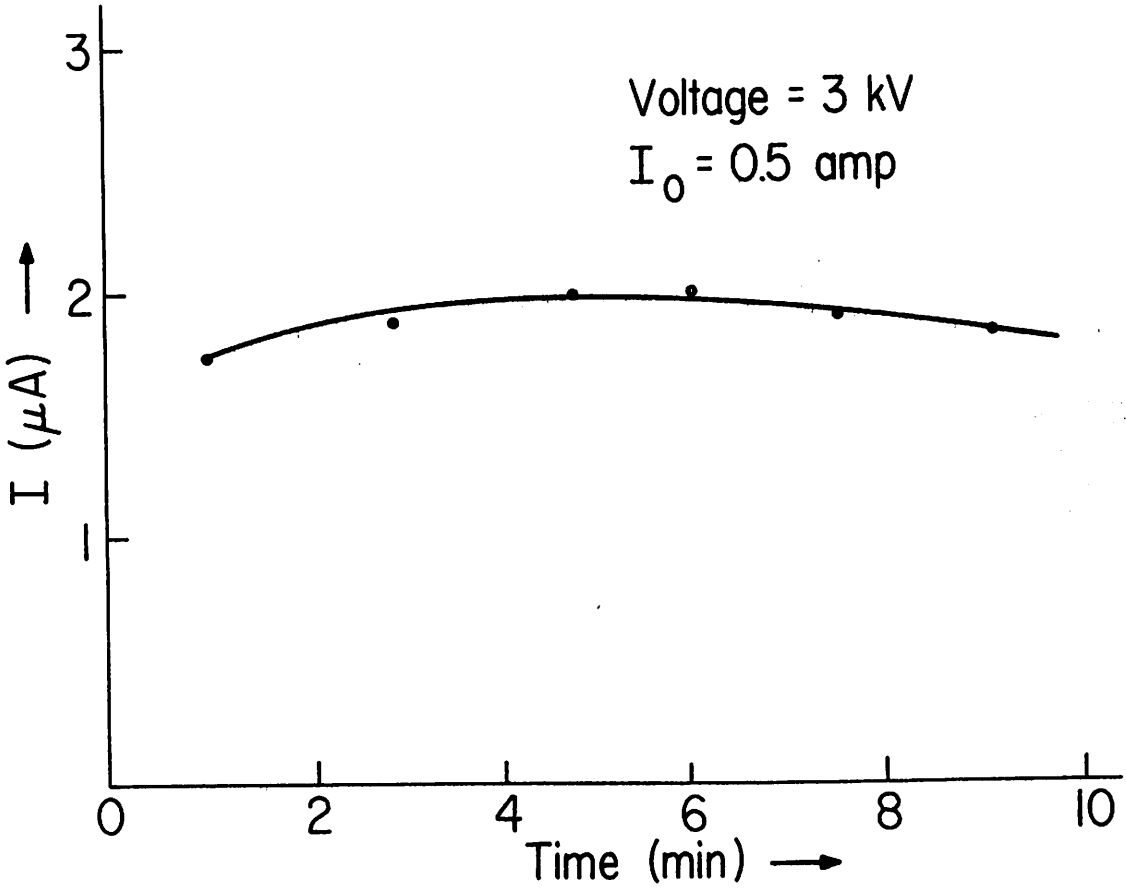

Fig. 29. Run 1, Current-time test of Tip F_3

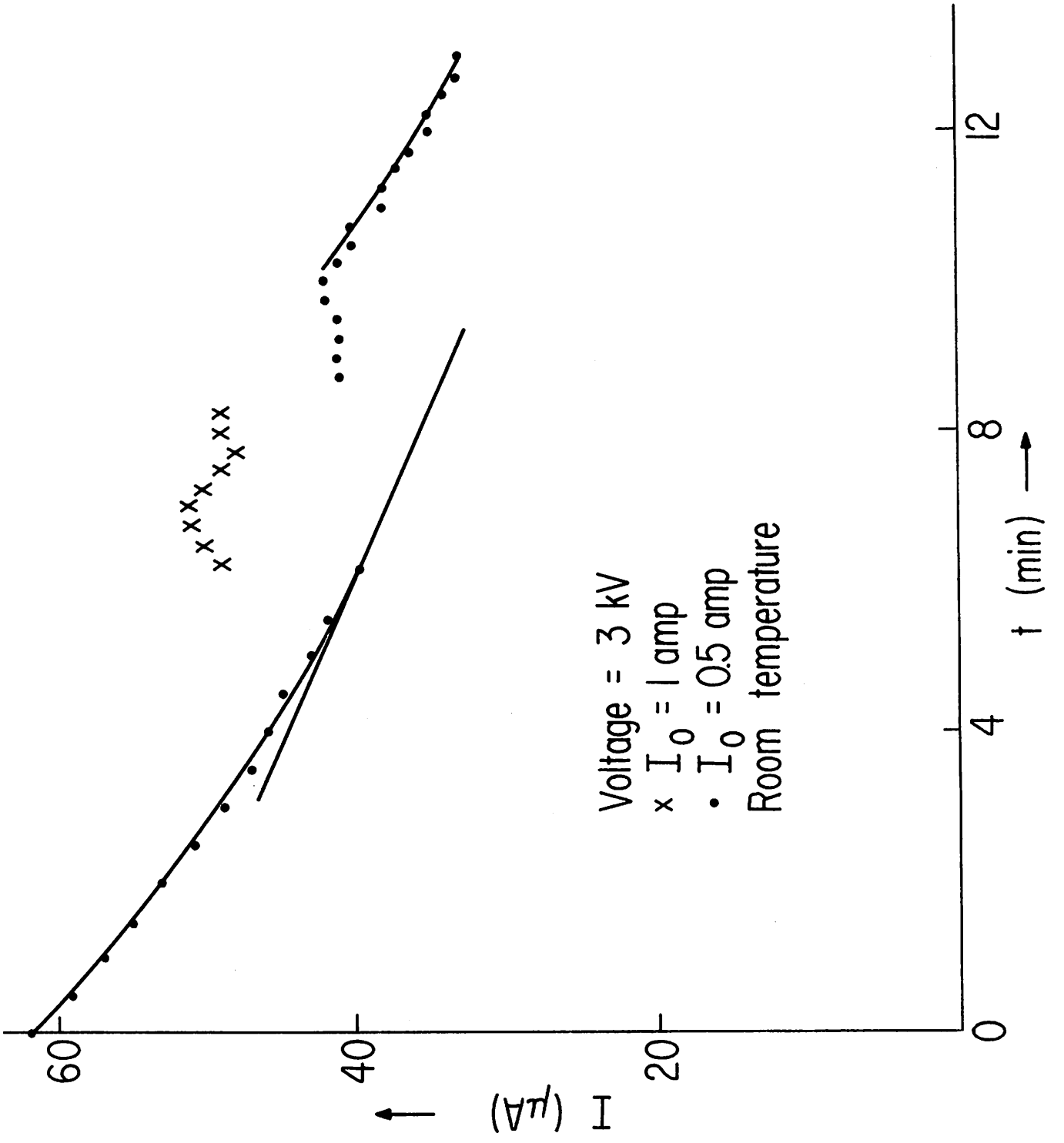

Fig. 30. Run 2, Current-time test (Tip F_3, no liquid N_2)

Summary

We have shown that a field-emission tip can be produced by electrolytic etching. The tip radius can then be approached by post-etching; the longer the post-etch pulse, the greater the radius. Four runs were made, each of a different tip. All four show rather good agreement with theory. Runs 3 and 4 show the variations that can result from changes in work function and tip radius. Current-time tests have been made which show the stability of emission, exhibit the effects of a poor vacuum, and indicate the possibilities of rejuvenating a tip by heating.

V. CALCULATIONS

Current-voltage calculations:

We recall that Eqs. 5 and 6 were

$$I = A_3 e^{-A_4/V} , \tag{6}$$

and

$$I = (A_1 A_e \beta^2 V^2/\phi_e) \exp\left[A_2 \phi_e^{3/2} f(y)/\beta V\right] . \tag{5}$$

Identifying like terms, we find

$$A_3 = A_1 \beta^2 V^2 A_e/\phi_e , \tag{9}$$

and

$$A_4 = -A_2 \phi_e^{3/2} f(y)/\beta . \tag{10}$$

Assuming ϕ_e and f(y) are constant, we define for convenience two new constants:

$$A_5 = A_1/\phi_e \ , \tag{11}$$

and $$A_6 = A_2\phi_e^{3/2} f(y) \ . \tag{12}$$

Substituting these into Eq. 5, we get

$$I = A_5 A_e \beta^2 V^2 \exp A_6/\beta V \ . \tag{13}$$

We take ϕ_e to be 4.5 eV, a value taken from thermionic measurements (1, p. 105). Also we take y to be 0.76; a value computed from Eq. 3 and typical values (1, p. 92, Fig. 1) of F, ϕ_e, and ϵ :

$$F = 5(10^7) \text{ V/cm}$$

$$\phi_e = 4.5 \text{ eV}$$

$$\epsilon = 1 \text{ eV}$$

Using y = 0.76 and the table of f(y) vs y (1, p. 93), we find

$$f(y) \cong 0.37 \ .$$

Substituting these values of ϕ_e and f(y) together with A_1 and A_2 (Eqs. 1 and 2) into Eqs. 11 and 12, we get

$$A_5 = 3.42(10^{-7}) \text{ amp/V}^2 , \tag{14}$$

and $$A_6 = -2.4(10^8) \text{ V/cm} . \tag{15}$$

Using Fig. 7 in reference 4 (p. 15), and a typical value of the electric field, we find

$$A_e \cong 1.5r^2 .$$

Also, we recall Eq. 7:

$$\beta = 1.7/(r^{0.87}R^{0.13}\alpha^{1/3}). \tag{7}$$

Substituting these values into Eq. 13, we obtain

$$I \cong 4.3A_5V^2(r/R)^{0.26}\alpha^{-2/3} \exp\left[-0.59A_6r^{0.87}R^{0.13}\alpha^{1/3}V^{-1}\right] . \tag{16}$$

Then, using R (cathode-anode distance) = 0.5 cm and Eqs. 14 and 15, Eq. 16 becomes

$$I \cong 1.76(10^{-6})r^{0.26}\alpha^{-2/3}V^2 \exp\left[-1.3(10^8)r^{0.87}\alpha^{1/3}V^{-1}\right] . \tag{17}$$

From Eq. 17 we see that I is most strongly affected by V due to its presence in the exponential term. Thus we can represent the coefficient of Eq. 17 as a constant with sufficient accuracy. In agreement with Eq. 6, we call this constant A_3. This simplification is justified

by the results. For example, in Fig. 27 we see that as 1/V varies from 0.4 to 0.6, I changes by a factor of 100, whereas A_3 varies as V^2. That is, A_3 changes by a factor of only 2.

In comparing Eqs. 6 and 17, we see that

$$A_3 \cong 1.76(10^{-6}) r^{0.26} \alpha^{-2/3} V^2 . \tag{18}$$

To represent A_3 as a numerical constant, values of r, α, and V must be substituted into Eq. 18. We will use the typical values:

$$V = 10 \text{ kV}, \quad \alpha = 10^{\circ}, \quad \text{and} \quad r = 7000 \text{ Å} .$$

A_3 then becomes:

$$A_3 \cong 3.2 \text{ amp.}$$

Finally, Eq. 17 can be rewritten as

$$I \cong 3.2 \exp\left[-1.3(10^8) r^{0.87} \alpha^{1/3} V^{-1} \right] . \tag{19}$$

Using Eq. 19 and the photographically estimated values of r and α, we find:

$$\text{for Run 3,} \qquad I \cong 3.2 \exp\left[-8.1(10^4) V^{-1} \right] , \tag{20}$$

$$\text{for Run 4,} \qquad I \cong 3.2 \exp\left[-4.4(10^4) V^{-1} \right] . \tag{21}$$

These equations are plotted along with the results of Runs 3 and 4 for comparison with these results.

Pressure Estimate (Run 1)

An upper limit estimate of the pressure of the vacuum obtained in Run 1 can be made using Eq. 8 and the current-time plot of Fig. 29.

Equation 8 is:

$$(1/I)dI/dt = 10^{11}pI^{0.7}$$

Solving for p, we find

$$p = 10^{-11}I^{-1.7}dI/dt. \tag{22}$$

Approximating Eq. 22:

$$p \cong 10^{-11}I^{-1.7}\Delta I/\Delta_t .$$

Choosing from Fig. 29 maximum values of ΔI and Δt, and an average value of I, we obtain

$$I_{av} \cong 1.9(10^{-6}) \text{ amp},$$

$$\Delta I \cong 0.3(10^{-6}) \text{ amp},$$

and $$\Delta t \cong 8 \text{ min} = 0.13 \text{ hr}.$$

Then $$p \cong 9.2(10^{-8}) \text{ torr}.$$

Pressure Estimate (Run 2)

An estimate of the pressure of the vacuum obtained in Run 2 can be made using Eq. 8 and the current-time plot of Fig. 30.

Equation 8 is

$$(1/I)dI/dt = 10^{11}pI^{0.7} .$$

Solving for p, we find

$$p = 10^{-11}I^{-1.7}dI/dt. \qquad (22)$$

Choosing values from Fig. 30 for I and dI/dt (for convenience at t = 0), we get

$$I_0 \cong 62 \text{ m}\mu\text{amp},$$

and $$(dI/dt)_0 \cong 2.88(10^{-7}) \text{ amp/hr.}$$

Then $$p_0 \cong 6.5(10^{-6}) \text{ torr.}$$

We note that if we choose I and dI/dt at t = 5 min, we find:

$$I_5 \cong 43 \text{ m}\mu\text{amp},$$

and $$(dI/dt)_5 \cong 1.78(10^{-7}) \text{ amp/hr.}$$

Then $$p_5 \cong 7.6(10^{-6}) \text{ torr.}$$

That these two values of p are so close indicates that the decay truly has the form shown in Eq. 22.

VI. CONCLUSION

Field-emission tips have been reliably fabricated. The tests of these tips exhibit results that generally agree with the theory. As regards the special requirements to be met for use of the tips in a scanning electron microscope, currents up to 1 μamp have been reached at voltages less than 3 kV and a significant fraction of this current is in the forward direction. The tips have also shown good stability over periods of ten minutes. Tests of stability over periods of several hours have, however, not been obtained; nor have tests been devised to show, more accurately, the peaking in the forward direction.

REFERENCES

1. W. P. Dyke and W. W. Dolan, Advances in Electronics and Electron Physics VIII, 89 (1956).

2. M. Drechsler, V. E. Cosslett, and W. C. Nixon, The Point Cathode As An Electron Source, Cavendish Laboratory, University of Cambridge (England).

3. R. A. Millikan and C. C. Lauritsen, Proc. Nat'l. Acad. Sci. (U.S.) XIV, 45 (1928).

4. E. E. Martin, H. W. Pitman, and F. M. Charbonnier, Linfield Research Institute, Astia Document AD210565 (1959).

5. E. E. Martin and H. W. Pitman, Linfield Research Institute, Astia Document AD202556 (1958).

6. W. R. Savage and F. J. Low, The Review of Scientific Instruments XXXV, No. 7, (1964).

7. W. P. Dyke, F. M. Charbonnier, R. W. Strayer, R. L. Floyd, J. P. Barbour, and J. K. Trolan, J. Appl. Phys., Vol. 31, No. 5, (1960).

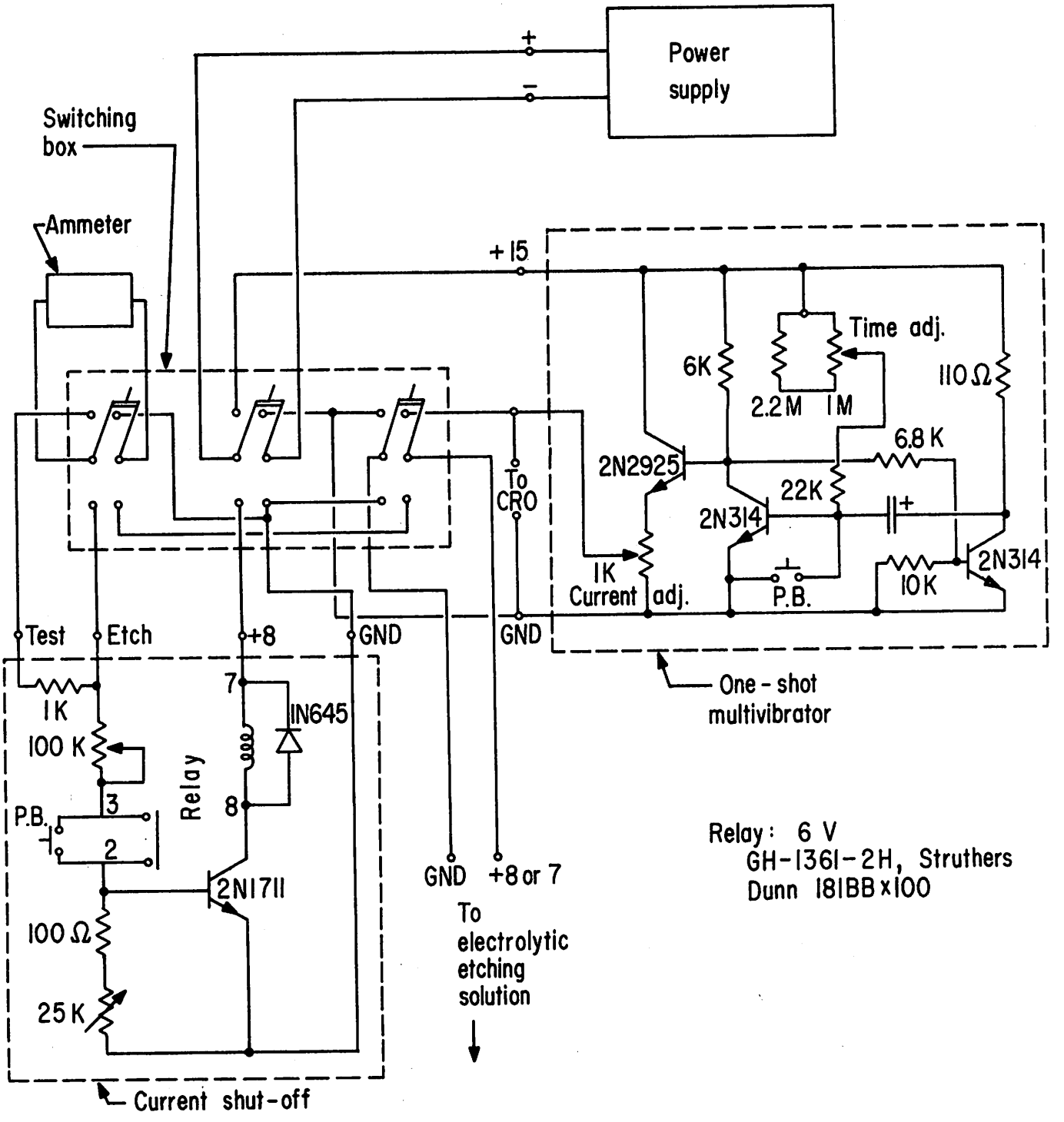

Current shut-off and one-shot multivibrator circuits